WRC RESEARCH REPORT NO. 13

MICROSCOPIC DETERMINATION OF BOUNDARY SHEAR AND SUBLAYER TURBULENCE CHARACTERISTICS IN AN OPEN CHANNEL

Harry G. Wenzel
Assistant Professor of Civil Engineering

Michael J. Mathews
Research Assistant

University of Illinois

FINAL REPORT

Project No. A-006-ILL

June 1, 1965 - June 30, 1967

The work upon which this publication is based was supported by funds provided by the U.S. Department of the Interior as authorized under the Water Resources Research Act of 1964, P.L. 88-379
Agreement No. 14-01-0001-907

UNIVERSITY OF ILLINOIS
WATER RESOURCES CENTER
3220 Civil Engineering Building
Urbana, Illinois 61801

January 1968

ABSTRACT

The application of a method of velocity determination in an open channel using a microscope and camera to record the motion of small particles suspended in water is described. Velocity measurements were made in a series of thin planes orientated parallel to the channel bottom for the case of two-dimensional laminar and turbulent open channel flow. Velocity profiles near the boundary were plotted and boundary shear computed from the rate of shear thus determined. Turbulence intensity was computed and the distribution of particle velocities examined.

It was concluded that the method yields boundary shear values to within $\pm$ 15 percent and that this uncertainty can be reduced significantly. The maximum error is caused by uncertainty in the location of the focal plane and in the location of a particle within the focal plane. This difficulty causes an even greater error in computation of turbulence intensity. This error increases as the distance from the boundary decreases, creating a serious disadvantage of the method. Particle velocity distributions exhibit a positive third moment which is in qualitative agreement with previous measurements.

The results indicate that further investigation of the application of the method to open channel turbulent flow is justified. It is planned to modify the method so that particle motion can be viewed in a plane orientated normal to the boundary. This will considerably reduce the primary errors described in this report and permit more accurate turbulence measurements very near the boundary.

CONTENTS

LIST OF FIGURES

LIST OF TABLES

NOTATION

A = cross sectional area of flow

C_L = lift coefficient

D = pipe diameter, depth of channel flow

d = particle diameter

$E_a(\ )$ = absolute error

$E_r(\ )$ = relative error

e = base of natural logarithm

ΔF = number of frames

F_L = lift force

i = index

j = index

m = mass, index

m' = index

N_R = Reynolds' number based on channel depth

N_{R_P} = particle Reynolds' number

n = index

Q = discharge

S = channel slope

Δt = time increment

U = settling velocity

$\bar{u}$ = average local velocity in x direction

u_i = instantaneous particle velocity in x direction

u_j = average particle velocity in x direction

u_p = particle velocity

u_y = velocity at distance y above channel bottom

u_τ = friction velocity = $\sqrt{(\tau_o/\rho)}$

u^+ = dimensionless local average velocity = $\bar{u}/u_\tau$

u' = velocity fluctuation in x direction

v = velocity in y direction

$\bar{w}$ = average local velocity in the z direction

w' = velocity fluctuation in z direction

x = direction of longitudinal axis of the channel

x_i = x coordinate of particle in frame i

y = normal distance from channel bottom

y^+ = dimensionless distance from channel bottom = yu_τ/ν

z = direction normal to x direction in the plane of the channel bottom

α = coefficient

γ = specific weight of water

γ_p = specific weight of a particle

μ = absolute viscosity, micron

ν = kinematic viscosity

ρ = density of water

ρ_p = density of particles

τ = shear stress

τ_o = shear stress at boundary

1. INTRODUCTION

The importance of knowledge concerning the boundary shear stress or tractive force in open channel flow has been recognized for some time. The capacity of a channel is directly related to the boundary shear. Although an average value may be readily computed for steady, uniform flow conditions using a static balance between gravity and shear forces, a thorough understanding of the complete flow pattern, including secondary flow characteristics, requires a knowledge of the boundary shear distribution. Knowledge of shear distribution is of great value in sediment transport. The application of the concept of critical tractive force requires a knowledge of the value of the boundary shear. Although present methods usually consider only average values, the knowledge in this area is continually being advanced, and there is little doubt that variation in boundary shear will ultimately be considered in design procedure.

The flow pattern in the boundary layer is generally a complex three dimensional unsteady problem which poses experimental difficulties in the measurement of boundary shear. There are two broad classifications of techniques for determining the shear. One is the direct measurement of shear force. This is usually done using a small element of the boundary which is isolated and instrumented to measure the force required to keep it in position in the presence of flow. The other is an indirect method in which the boundary layer velocity profile is measured by some means which is then related to boundary shear using Newton's law of viscosity.

The purpose of this study is to investigate the feasibility of using an optical technique to measure the velocity distribution in the sublayer region and, from this data, obtain the boundary shear stress. In essence the technique employs a microscope to view the motion of small particles suspended in the flow. The particles act as tracers and thus at any instant their velocity is identical to the fluid velocity vector at that point. The motion is recorded on film and the distance traveled over a short time interval is divided by the time interval to yield a velocity approximation which approaches the instantaneous velocity as the time increment becomes small. Thus, turbulent fluctuations as well as average velocity can be measured if the time increment is sufficiently small. Because the field of view of the microscope is very small, the results can be considered as a point measurement except in the lower portion of the sublayer. By locating the plane of focus with respect to the boundary the position of the velocity measurement can be determined and, by examining the flow over a range of depth, the velocity profile can be established.

The method has the advantage of not requiring the insertion of a probe into the flow. It also is a direct method of velocity measurement since the only calibrations required are time and space if the particles act as true tracers. It has the disadvantage of requiring considerable time and effort to reduce the data from the film.

This report describes in detail the apparatus, procedure, results of some initial tests, and preliminary evaluation of the method based on a two dimensional flow situation with the optical plane of

focus orientated parallel to the channel boundary. A second phase of the study is underway in which the boundary shear distribution will be investigated with the plane of focus orientated normal to the boundary.

The work upon which this publication is based was supported in part by funds provided by the U. S. Department of the Interior as authorized under the Water Resources Research Act of 1964, P.L. 88-379. The experimental work was performed in the Hydraulic Engineering Laboratory of the Department of Civil Engineering.

The authors wish to express appreciation to Bauer Engineering, Incorporated who undertook the design and construction of the channel, to Professor H. M. Karara of the Department of Civil Engineering for permitting the extensive use of the optical comparator, and to Professor J. W. Westwater of the Department of Chemistry and Chemical Engineering for the use of the film analyzer. Also, discussions with Dr. Paul Bock, Travelers Research Center, and Professor Charles E. Carver, University of Massachusetts, were of considerable help in avoiding many of the experimental pitfalls associated with the adaptation of the microscope system.

2. REVIEW OF PREVIOUS STUDY

2.1 — Velocity Measurements Employing a Microscope

The microscopic technique was pioneered by Fage and Townend[1*] in 1932. They observed the particles in ordinary tap water flowing in a square brass pipe of 0.89 in. side dimension. Turbulent velocity fluctuations were observed using a rotating lense system but no photographs were taken. In 1936, Fage[2] reported observations of turbulent flow in a 1.064 in. diameter round tube. Again no photographs were taken. One year later, Vogelpohl and Mannesmann[3] published the results of quantitative velocity measurements in the laminar and transition region. A light interrupter disk was used to obtain streaks on a photograph and fine aluminum particles were used as tracers. Flow patterns were studied in the entrance and fully developed sections of a circular pipe. Fage has employed the ultramicroscope to make additional studies. In 1941, work with Preston[4] was reported in which the boundary layer transition from laminar to turbulent flow was studied. Again, in 1955, Fage reported additional studies of boundary layer flow[5].

Several studies, reported in the past five years, have resulted from a renewed interest in boundary layer flow and from the improvement of microscopic equipment. Bock[6] used polystrene latex spheres in a study of laminar flow in a small rectangular duct. He photographed their motion with 35 mm camera, using a time exposure, to obtain streaks from which the velocity could be determined. Much of the microscopic equipment used in the present project is similar to that used by Bock. He

---

*Superscript numbers refer to reference list.

made velocity measurements to within 10 microns (μ) of the boundary and verified the interesting and yet unexplained sinuous motion reported by previous investigators. The method was first used for open channel flow by Vasuki[7] who measured velocity profiles of laminar flow with depths of 80 to 120 μ. Using equipment similar to Bock's, Carver[8] measured velocity profiles of laminar flow of water in a rectangular tube with, and without, non-Newtonian additives. Carver used a rotating disk to interrupt the light source, producing a series of streaks on 35 mm and Polaroid film.

A method which could yield valuable results with turbulent flow was developed by Chen and Emrich[9] and used by Elrick and Emrich[10] for laminar flow studies of air in a rectangular tube. The basic difference between this method and previous ones is that the microscope or camera system is positioned such that the particle and its mirror image as reflected from the pipe boundary are both recorded on the film. Thus, motion in a plane normal to the boundary is recorded and the boundary is located on the film equidistant from the particle and its image. Elrick used smoke particles less than 0.1 μ in diameter and obtained velocity measurements as close as 2 μ to the boundary. He observed, as have others, fluctuations in particle motion which cannot be explained by Brownian motion. Furthermore, unexplained irregularities in the velocity profile near the boundary were measured which indicated an apparent wall slip. It is presently planned to adopt this idea in the second phase of the current study to measure the velocity profile for turbulent flow in a plane normal to the channel wall.

It should be noted that this review is concerned only with studies which have used tracers of microscopic size which require magnification for reviewing. There have been numerous studies made with a variety of larger size tracers but their value lies in revealing macroscopic flow patterns rather than the fine details of flow very near a boundary.

2.2 — Turbulence Measurements in the Viscous Sublayer

The concept of a laminar sublayer was proposed as early as 1916 by Taylor and supported by Stanton. This early picture of a layer of purely laminar flow has since been modified as a result of recent advances in experimental technique which permit measurements to be made relatively close to a boundary. These studies indicate that fluctuations do exist in the sublayer and hence it should be more properly termed the viscous sublayer.

In 1951 and 1954, Laufer[11, 12] and in 1955, Klebanoff[13] reported extensive hot-wire anemometer measurements of air turbulence characteristics in the outer region of the sublayer. Laufer's first study concerned two-dimensional flow in a rectangular channel. Mean velocity and all three fluctuating components were measured. Turbulent intensity, shear, correlation coefficients, scales of turbulence, and energy spectra were computed. In Laufer's later report, similar quantities were computed for air flow in a 10 in. diameter pipe. Klebanoff's measurements were performed in a 4.5 ft wind tunnel with zero pressure gradient. He reported the probability density of the fluctuation in the direction of flow in addition to the usual statistical parameters.

A series of studies performed at Stanford University[14, 15] used hot-wire and hot-film measurements in water. Velocity data was obtained to within a wall Reynolds number, y^+, of 0.5[15]. In addition, a hydrogen bubble technique was effectively employed for visualization of the eddy structure and measurement of velocity.

In order to avoid some of the problems associated with the use of hot-wire probes very close to a boundary Bakewell[16] used glycerine as a working fluid. A sublayer thickness of approximately 0.1 in. was developed and detailed hot-film measurements were made to within $y^+ = 1$. The study was restricted to streamwise velocities.

A unique electrochemical technique has been developed by Hanratty[17] which is capable of measuring velocities very close to a boundary, $y^+ < 0.5$. The method consists essentially of an electrode which is mounted flush with the boundary. The working fluid is an aqueous solution of potassium ferricyanide. By applying a voltage to the electrode a chemical reaction is initiated. The resulting current in the circuit is related to the rate of mass transfer at the electrode which is in turn related to the velocity near the boundary. This method has the advantage of not disturbing the flow with a probe but presents calibration problems as does the hot-wire method.

The most recent study by Tieleman[18] employed rotated hot-wire measurements of a 32 in. thick boundary layer in a wind tunnel. Velocities were measured to within $y^+ = 1$ and statistical parameters were computed. The report contains a valuable discussion of calibration procedures and errors associated with turbulence measurements in a shear layer near a boundary.

The preceding summary of sublayer research is not complete but mentions the most significant studies. A general conclusion is reached that no single method is clearly superior for measurements close to a boundary. Each has limitations and, since knowledge of this region of flow is now recognized as essential, the pursuit of the optical method reported here is of value.

3. APPARATUS

3.1 — Flow System

The flow system consisted of a specially designed open channel, centrifugal pump, filter, and orifice meter. The channel, shown in Fig. 1, was rectangular with a 6 in. by 1 in. cross section and was 10 ft long. The bottom and sides were constructed of 0.25 in. thick plate glass. The bottom was supported by a series of 6 in. by 10 in. glass support plates which in turn rested on pairs of adjusting screws mounted on 6 in. centers along the channel. The screws were in turn threaded through the top flange of a specially fabricated 9 in. deep aluminum support beam which can be seen in Fig. 2. This system provided an extremely rigid support for the channel and minimized slope variations. The head box and tail box were the same width as the channel and fabricated as part of the support beam. The beam was pivoted at the downstream end, and the slope was adjusted by means of a screw system at the upstream end. A dial gage attached to the head tank permitted the slope to be set to within 0.001 percent. The channel supports rested on concrete pads which in turn rested on rubber pads to effectively isolate the system from floor vibrations. The water was recirculated using a 5 gpm centrifugal pump which was mounted on the floor and connected to the system through flexible hoses which prevented vibrations from being transmitted to the channel. Copper or vinyl tubing was used throughout to prevent rust. Flow rate was determined using a calibrated orifice meter located in the return line to

the head box. The flow was regulated by a gate valve and a bypass line with a needle valve, which provided very sensitive and stable control. A filter capable of removing particles greater than 5 μ in diameter was placed in the system; however, the filter was bypassed during an actual test.

Polystyrene latex spheres supplied by Dow Chemical Company were used as tracer particles. Statistical data supplied by Dow states that the particles have an average diameter of 1.099 μ with a standard deviation of 0.0059 μ based on 106 measurements. Their specific gravity was 1.05 and they were supplied in a 10 percent solid suspension, deionized water being the suspending fluid. About 15 drops were added to the 15 gal. of distilled water in the flow system resulting in a final solid concentration of about 0.0025 percent.

3.2 — Microscope System

The microscope used in the experiments was a commercial Leitz Laborlux II, shown in Figs. 2 and 3. The entire upper optics of the microscope was adjustable by means of a micrometer screw calibrated in 1 μ division. The microscope was mounted in an inverted position on an adjustable steel plate which was supported by a steel frame, shown in Fig. 1, which rested on the floor. A 150 watt zenon lamp mounted in a housing on the steel mounting plate composed the illumination system. The lamp was focused through a 45 degree mirror onto a Leitz DO.45 darkfield condenser, located above the center of the channel as shown in Fig. 2. The condenser focused the light into a hollow conical

beam. By adjusting the vertical position of the condenser, the apex of the cone of light was focused at the point of interest in the flow. If a particle traveled through the plane of focus, light was reflected into the microscope lens, otherwise the light continued on its conical path and did not enter the lens. This provided a dark field of view with particle images appearing as bright spots somewhat larger than the actual particles.

The optical system consisted of either a 32x or 50x primary lens and a 10x eyepiece mounted in the optical tube. The depth of field of 50x lens was experimentally found to be about 11 μ and that of the 32x was 24 μ. The higher magnification lens was used primarily for measurements within 100 μ of the boundary because of its smaller depth of field while the 32x lens was used beyond this distance because it produced a sharper image and because the larger depth of field was not a serious disadvantage.

The microscope was mounted in an inverted position over the center line of the channel so that the particle image would pass through the glass channel bottom rather than the free surface, since small surface disturbances would refract the image causing apparent motions. Since the optical adjustment system was gravity driven, the inverted mounting position required the installation of a spring and clamp arrangement, seen in Figs. 2 and 3, which provided an upward force to hold the optics in position.

The location of the plane of focus was set using the micrometer screw on the microscope. However, it was found that the calibration was not exact so a dial gage was mounted between the optical tube of the

Fig. 1 — Channel

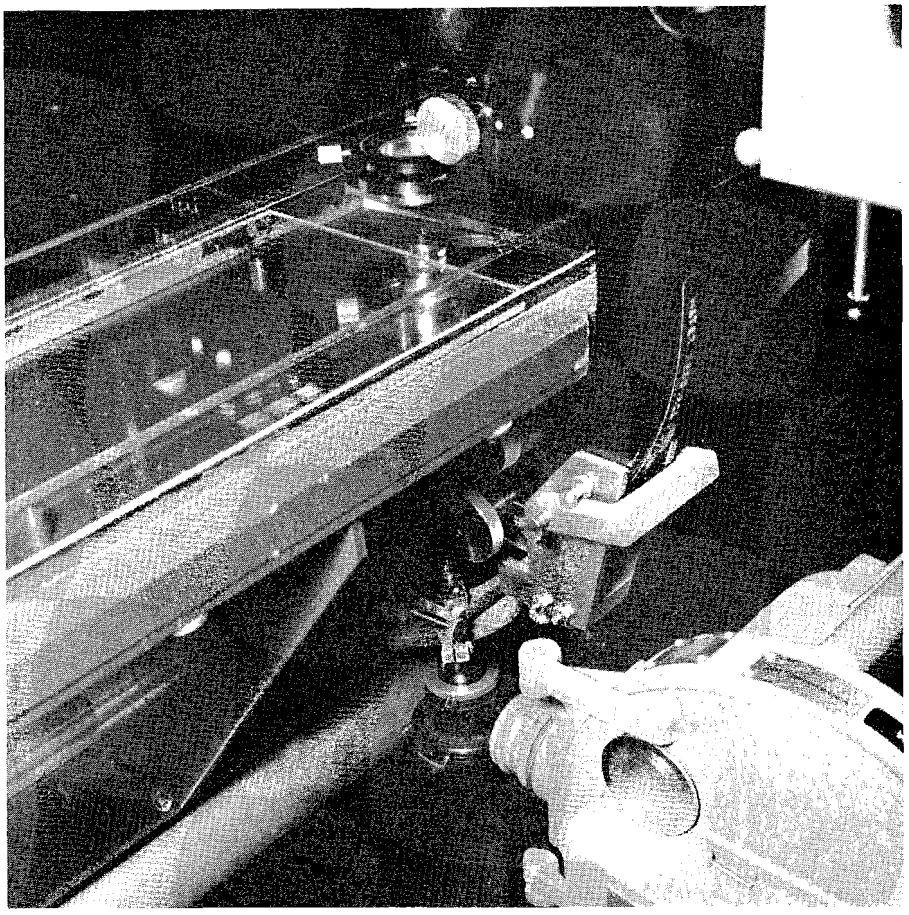

Fig. 2 — Microscope

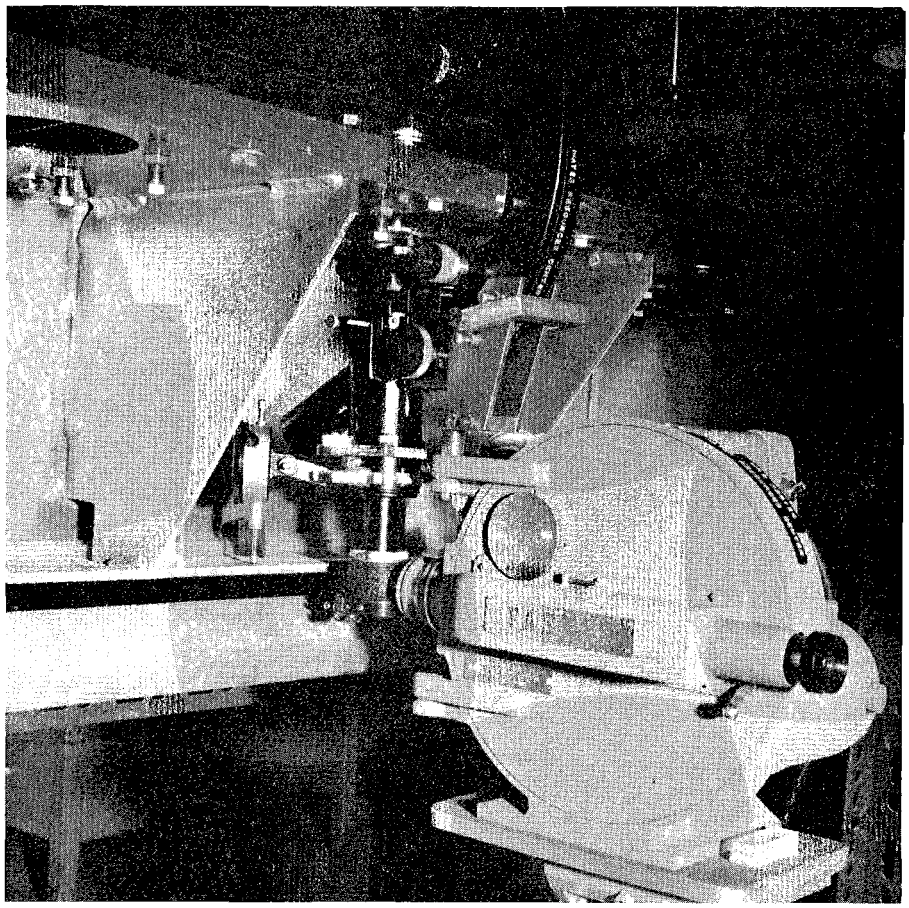

Fig. 3 — Microscope and Camera

microscope and the channel support beam as shown in Fig. 3. The gage was calibrated in 12.5 μ divisions and interpolated to 2.5 μ. This gage was used in conjunction with the micrometer screw reading to determine the location of the plane of focus.

Two types of cameras were used to record the particle motion. Preliminary studies of laminar flow were made using a 35 mm Leica M-3 camera body mounted on a microphotographic attachment consisting of a focusing telescope, a lateral viewing tube with a deflecting prism and a anti-vibration bayonet mount. A 12 in. diameter transparent rotating plexiglass disk with alternate sectors blacked out was used to chop the light, creating a series of particle streaks on the film. By using various disk patterns and rotational speeds, an optimum streak pattern for each velocity could be obtained. Tri-x film was used and developed in the laboratory at an effective ASA rating of 2400.

Turbulent flow data was recorded using a 16 mm Fastax high speed motion picture camera with a 100 ft film capacity and a 50 mm lens. The camera was mounted on a tripod and driven by a control unit, both shown in Fig. 1. The particle image was transmitted into the lens through a lateral observation tube containing a deflecting prism and observed through the cameras viewing system. The camera lens was positioned very close but not in contact with the observation tube, thereby preventing camera vibrations from being transmitted to the microscope. Camera speeds of 1000 to 5000 frames/sec were used. To provide a fixed reference system on the film a cross-hair disk was mounted in the microscope tube and the background illuminated by permitting a small amount of light to pass directly through the darkfield condenser. The cross-hair was aligned

parallel and normal to the channel center line. All particle motion was computed with respect to the cross-hair reference system which effectively eliminated errors due to vibration since the vibrations of the channel and microscope were negligible. A 1000 cycle/sec timing pulse was imposed on the edge of the Kodak Tri-x 16 mm negative film. The pulse was generated by 1000 cycle per sec Nand Frequency Standard which, when amplified, fired the neon lamp in the camera. The high frequency pulse was required since the film was constantly being accelerated as it was exposed causing the time interval between frames to vary through the film.

3.3 — Data Reduction System

The process of data reduction for the turbulent flow experiments consisted of three phases: (a) the establishment of a time interval between frames on the film, (b) the recording for each frame the co-ordinates of the particles to be examined and (c) the combination of this information to compute velocities and statistical turbulence parameters.

The time calibration was accomplished using a L.-W. Photo Analyst projector capable of advancing the film frame by frame. The procedure is described in Chapter 4. The particle co-ordinates were recorded using two instruments which provided an accurate and relatively rapid means of accomplishing this formidable task. The first was a Wild Optical STK-1 Comparator, an instrument designed for photogrammetry work. It was equipped with a optical reference point and when set, the rectangular co-ordinates and any associated numerical data desired were typed on paper and punched and printed onto computer cards. Since the comparator

was designed for stereo map reading, a special film transport mechanism was constructed so the film could be used directly without projection. The second instrument used was a Vanguard film analyzer which projected the film on a screen. Cross hairs were placed over the particle and the co-ordinates recorded on paper tape along with the frame number. The data was subsequently transferred to computer cards.

Reduction and analysis programs were written and all information was processed on the University IBM 7094 system.

4. EXPERIMENTAL AND ANALYSIS PROCEDURES

4.1 — Test Preparation

Preparations for the laminar and turbulent flow tests were essentially the same. The channel was placed at zero slope according to the dial indicator and filled with distilled water to the depth anticipated in the test. The bottom was then precisely leveled laterally and longitudinally by means of the adjusting screws. A 60 sec. per division striding bubble level with a 5 in. span was used as a level indicator.

The pump was started and the water allowed to recirculate through the system and filter to bring the temperature to equilibrium and to filter out foreign particles. The desired flow rate was set according to the orifice meter manometer reading and the proper channel slope set. The magnitude and uniformity of depth was checked with the micrometer point gage. Minor changes in the slope and adjustments of a skimming wier in the downstream tank were made until the depth was uniform in the region of the test section which was 6 ft from the channel entrance. At this point the boundary layer from the bottom was fully developed but development from the sides had not reached the center of the channel.

The flow was then allowed to bypass the filter and the flow rate adjusted to compensate for the removal of the filter head loss. About 15 drops of the tracer solution were added to the water at the tail box and allowed to mix uniformly with the flow. Minor adjustments were made until no change in depth over a one-half hour period was noted.

4.2 — Laminar Flow Tests

For these tests a 35 mm camera was used in conjunction with a rotating disk to produce streaks of known length. The camera was loaded with a cassette of Tri-x film and attached to the microscope camera adapter. The microscope was focused on the bottom of the channel bottom and the zero reading was recorded from the micrometer screw and from the dial gage. The light-chopper disk was started and allowed to attain a steady speed. The rotational speed of the disk was recorded either by a stop watch or by a low speed stroboscope.

The microscope was raised a predetermined distance by the micrometer screw and the readings recorded from both the micrometer screw and from the dial gage. The dark field condensor was adjusted for optimum illumination of the field of view. A series of frames were exposed by opening the camera shutter for a long enough period to obtain a number of streaks. The 50x objective was used in the lower 100 μ region because of its smaller depth of field. The 32x lens was used above this level where its greater depth of field was of less significance since it produced a sharper image.

Pictures were taken at various selected levels until the surface of the flow was reached. Typical photographs are shown in Fig. 4. The surface was located as closely as possible, and a series of pictures were taken at small distances from the surface. At the completion of the test the depth, temperature, flow rate, and disk speed were again recorded. The pump was stopped and calibration pictures were taken of the stage micrometer with the 50x and 32x lenses.

The film strips were developed using Bauman Diafine Developing solution to yield a greater sensitivity than by the standard developing methods. The negatives were marked along the edge with their corresponding identification numbers. Enlarged prints of the particle tracers and scale were printed to the same scale on 4 x 5 inch projection paper.

The streak lengths of the particle images were measured to within 0.02 in. from the prints or to 2 mm from the projected image of the film negative. The accuracy of measurement was approximately the same for both methods due to the error in determining the end points of the particle streak. Where possible the streak length was established over two or more streaks of the same particle and averaged. All of the in-focus particle streaks appearing in each frame were measured.

The scale was determined from the photographs of the scale for the 50x and 32x lenses. The measured streak lengths were converted to true distance in the flow field in microns using the calibration from the photographs of the scale. The time increment for a streak was calculated by dividing the average streak length by its corresponding computed time interval. The velocity point was located on the profile plot at the center of the depth of field as determined from the corrected micrometer screw and dial gage readings.

4.3 — Turbulent Flow Tests

After the desired flow conditions were achieved and recorded, the microscope was focused so that the channel bottom was near the upper limit of the plane of focus. This was used as the zero depth position

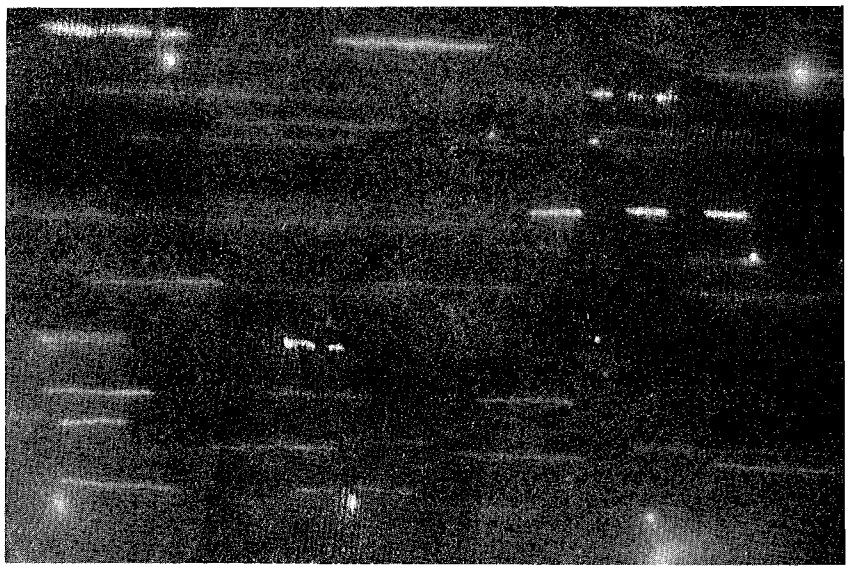

y = 11 μ u = 28 μ/ sec

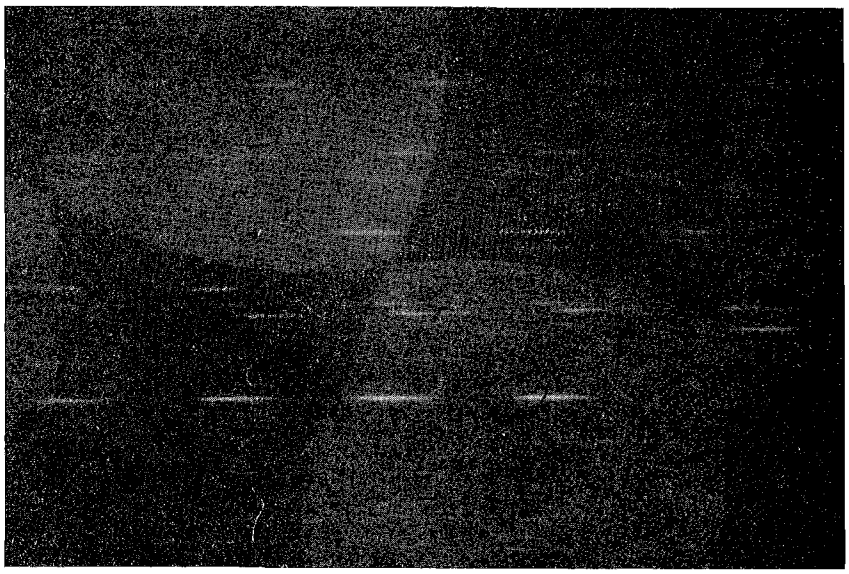

y = 2,278 μ u = 5,450 μ/sec

Fig. 4 — Laminar Flow Streak Photographs

and the dial gage and micrometer adjusting screw position on the microscope was noted. The microscope was then raised a predetermined distance using the micrometer screw, and its reading as well as that of the dial gage were recorded. The dark field condenser was adjusted for optimum contrast. A 100 ft roll of film was then placed in the camera, the desired speed set on the camera control unit, and the film exposed.

This procedure was followed until it was desired to change the objective. At this time the depth and flow rate were checked. The 50x lens was used primarily for measurements near the boundary and the 32x lens was used in the upper regions of the sublayer. The microscope was focused on the bottom as before and the procedure repeated. At the completion of the test series the depths and flow rate were again recorded.

At the completion of the test a film was taken using the high-speed camera of a stage micrometer placed on the channel bottom. The micrometer contained a scale 1 mm long with 10 μ divisions. Films using the 32x and 50x lens were taken and used for calibration purposes.

4.4 — Data Reduction

The data reduction procedure consisted of three phases: (a) determination of a real time calibration of the film on a frame by frame basis, (b) establishment of the coordinates of the particles judged to be in focus, and (c) computation of the velocity of each particle between two successive frames.

The time calibration was based on the 0.001 sec interval timing marks placed on the edge of the film during exposure. The Kodak Analyst

projector was modified slightly to permit viewing of the entire edge of the film. The film was projected onto a screen upon which a sheet of rectangular grid paper had been attached. The distance from the projector to the screen was carefully adjusted so that the frame could be conveniently and precisely divided into 100 even divisions. The frame number and decimal fraction of the beginning of each successive timing pulse was recorded and subsequently punched on computer cards. A simple program was written to check the recording and punching operations. The input to this program consisted of a tabulation of the positions of the beginning of each timing streak on the side of the film in terms of the frame number to hundredths of a frame. If the time mark fell on a sprocket hole the corresponding entry was a blank on the card. The missing frame numbers due to unreadable time marker positions were interpolated from adjacent entries. Frame numbers and increments between the frame numbers of timing works were printed out by the program. The tabulation was visually scanned to detect errors and the original timing data was corrected. Quite often several runs were required to eliminate all of the errors.

The co-ordinates of the particles on the film were obtained using two similar instruments. The Wild STK-1 Comparator was used to analyze the majority of the films for the co-ordinates of the particles. A film advance mechanism constructed from an old projector was used to advance the film frame by frame over the plate of the Comparator. The mechanism was attached to the Comparator table. A "zero" frame was selected if the film had not already been timed. The film was advanced until it was smoothly operating and the "zero" frame was within the field

of view. The frame counter was set to zero. The Comparator table was then rotated so that its axes corresponded with the superimposed axes on the film. The film was observed by the operator to determine whether a particular frame contained any particles judged to be in focus. If a particle appeared which was in focus the operator entered the frame number from the frame counter onto the keyboard connected to the Comparator. An optical reference point in the plane of focus was aligned over the intersection of the reference axes on the film and the "record" button was pressed causing the coordinates of the reference system and frame number to be punched onto a computer card. The coordinates of the particle were recorded in the same way. The film was then advanced one frame, the frame number incremented on the keyboard and the reference and particle coordinates obtained. This procedure was repeated until the particle either passed out of the framing area or passed out of focus. The film was advanced until another in-focus particle appeared and the process repeated. Only one particle was followed at a time in order to help eliminate weighting of turbulence data.

In addition to the use of the comparator, some films were analyzed on the Vanguard film analyzer. The analysis procedure was essentially the same as on the comparator except for two differences. The frame number was automatically recorded by the machine without the necessity of transfer from the counter to a keyboard. The data, consisting of the frame number and coordinates, were tabulated on paper tape by means of a calculator wired into the analyzer. It was then necessary to punch the data onto computer cards for analysis on the computer.

The main program was developed to combine the timing data and the coordinate data and to calculate and punch a deck of cards containing: the (1) instantaneous velocities in the axial direction, u, and perpendicular to the axis of the channel parallel to the bottom, w; (2) the frame numbers; (3) time from beginning of the film; and (4) the incremental time between frames. A flow chart is shown in Fig. 5. The actual calculation of the velocities consisted merely of dividing the distance traveled by a particle by the incremental time and multiplying by a scale factor. It is necessary, however, to mention briefly some of the internal methods and assumptions used.

The input timing data was smoothed to reduce reading errors and errors due to possible slight variations in the flashing rate from flash to flash. It was assumed that the speed of the film varied smoothly and that for small increments of time the actual speed curve was linear. Therefore, the smoothing procedure consisted of the fitting of a least squares line through groups of three adjacent points and using this line to adjust the value of each point. Such a smoothing routine was carried out twice although in most cases the second smoothing proved to be unnecessary. The smoothed matrix of timing values, consisting of the frame position for each thousandth of a second marker, was converted into a matrix containing the time for the beginning of each frame by linear interpolation between two adjacent values in the smoothed array. The coordinate data was then read into the computer as pairs of coordinate sets. The velocities were then calculated and the results punched onto cards.

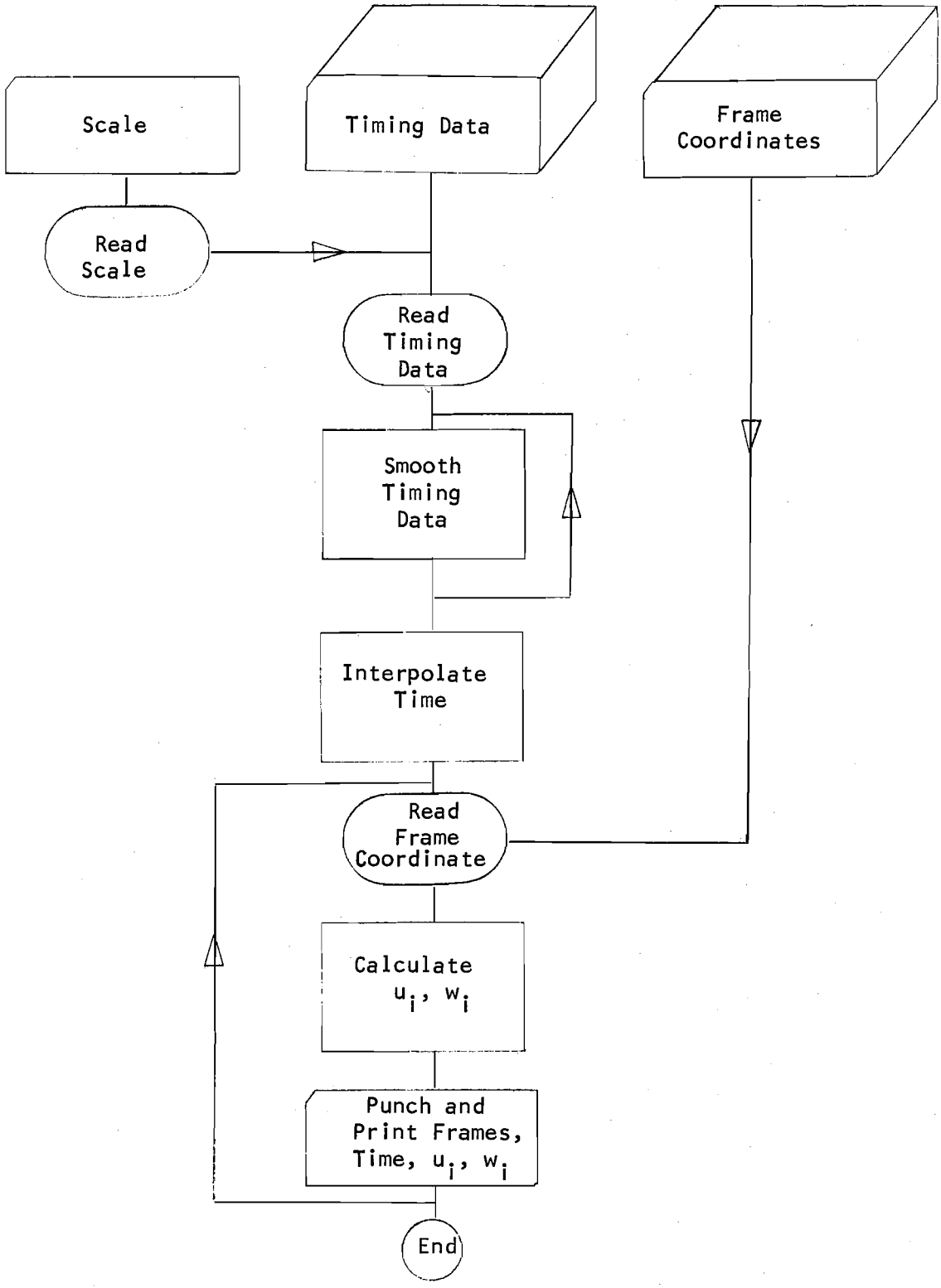

Fig. 5 — Main Program

4.5 — Data Analysis

The output of the main program was used as input to a group of programs which computed mean velocities, turbulence intensities and statistical distributions of mean velocities. The data from all films taken at any one level in the flow were analyzed individually. Since films at a given level contained different numbers of particles, separate analyses permitted comparison of the results obtained with various sample sizes.

The mean velocity was computed in two ways. In the first method the total net distance traveled by all the particles which were followed was divided by the total elapsed time in traveling that distance. This has the disadvantage of permitting the slower particles to influence the result more than the faster particles. The procedure is expressed by

$$\bar{u}_l = \frac{1}{\sum_{1}^{m} \Delta t_i} \sum_{1}^{m} u_i \Delta t_i \qquad (1)$$

where $\bar{u}_l$ = average velocity in the longitudinal direction, u_i = instantaneous particle velocity computed from two successive frames, Δt_i = time increment between frames used to compute u_i, and m = total number of instantaneous particle velocity values. The second method gives equal weight to the average particle velocity computed from

$$u_j = \frac{1}{\sum_{1}^{m'} \Delta t_i} \sum_{1}^{m'} u_i \Delta t_i \qquad (2)$$

where u_j = average velocity of particle j and m' = total number of u_i values computed for particle j which is equal to the number of frames over which the particle was followed minus one. The second equation for velocity then is

$$\bar{u}_2 = \frac{1}{n} \sum_{1}^{n} u_j \tag{3}$$

where n = total number of particles. In the same way values of the lateral average velocity, $\bar{w}_1$ and $\bar{w}_2$, were calculated.

With the average velocities known, the turbulence intensity was computed, again in two ways. The first way employed Eq. (1) to compute $\bar{u}_1$.

$$\overline{u_1'^2} = \frac{1}{\sum_{1}^{m} \Delta t_i} \sum_{1}^{m} (\bar{u}_1 - u_i)^2 \Delta t_i \tag{4}$$

where u' = turbulent fluctuation and thus $\overline{u'^2_1}$ = the square of the intensity in the longitudinal direction. The other symbols are as defined previously. The second method used $\bar{u}_2$ as defined by Eq. (3)

$$\overline{u_2'^2} = \frac{1}{n} \sum_{1}^{n} (\bar{u}_2 - u_j)^2 \tag{5}$$

Although of not as great an interest as the previous quantities, cross correlations between u' and w' were computed in two ways according to

$$\overline{u'w'_1} = \frac{1}{\sum_{1}^{m} \Delta t_i} \sum_{1}^{m} (\bar{u}_1 - u_i)(\bar{w}_1 - w_i)\Delta t_i \tag{6}$$

$$\overline{u'w_2'} = \frac{1}{n} \sum_{1}^{m} (\bar{u}_2 - u_j)(\bar{w}_2 - w_j) \tag{7}$$

Finally, the distribution of the longitudinal particle velocities was calculated, and from this the third moment or skewness, $\overline{u'^3}/(\overline{u'^2})^{3/2}$, was computed.

5. ERROR ANALYSIS

5.1 — Errors in Basic Data

The basic data used in the computations were the coordinates of the particles, the time interval between film frames, the scale factor and the position of the plane of focus with respect to the channel bottom.

The instruments used to record the particle coordinates were extremely accurate. The comparator could record an unmagnified length to within 1 μ and the analyzer to within .0001 in. This instrument error is negligible in comparison to the operator error in judging the center of the particle image. The reading errors were estimated by rereading the same point on the film a number of times for both series on both the comparator and the analyzer. The error in rereading was estimated to be about $\pm$ 5 units on the analyzer and about $\pm$ 18 units on the comparator. The corresponding absolute error in the position of a particle in the flow field is given below.

Lens	Analyzer Error
50x	$E_a(x_i) = 0.75 \times 10^{-6}$ ft = 0.23 μ
32x	$E_a(x_i) = 1.21 \times 10^{-6}$ ft = 0.37 μ
	Comparator Error
50x	$E_a(x_i) = 1.04 \times 10^{-6}$ ft = 0.32 μ
32x	$E_a(x_i) = 1.70 \times 10^{-6}$ ft = 0.52 μ

Error in the time increments was the result of the errors in interpreting the timing marks along the side of the side of the film and

the precision of the timing marks themselves. The flashing rate of the timing light was assumed to be accurate at 1000 pulses/sec. The error involved in determining the frame positions of the timing pulse was estimated to be about $\pm$ 0.01 of a frame. The resultant time error per frame was then

$$E_a(t) = \frac{.01(10^{-3})}{\Delta F} = \frac{10^{-5}}{\Delta F} \text{sec} \tag{8}$$

where $E_a(t)$ = absolute error in t and ΔF = number of frames between consecutive pulses. The frame-time values were smoothed in the analysis procedure and the error was presumably lessened in this manner.

The length scale was established on the comparator and analyzer by viewing the films taken of the stage micrometer using both the 50x and 32x lenses. The dimensions of the field of view were 250 μ long by 120 μ wide for the 32x lens and 150 μ long by 80 μ wide for the 50x lens. Thus, the stage micrometer, having a total calibration length of 2000 μ, filled the field. This permitted the scale to be checked at various points throughout the field. The scale factor was found to be constant. The scale length was 8,400 units on the comparator which, when compared to the maximum reading error of 36 units, yields a maximum relative error of 0.42 percent for a single determination. The corresponding error for the analyzer was 0.64 percent. The error in the final scale factor was less, however, since the average of 20 determinations on the comparator and 5 on the analyzer were used for the determination.

The position of the focal plane in the flow was located as described in Chapter 4. The readings were corrected by a factor of 1.33

for the ratio of refractive indexes of air and water. This factor was checked by measuring the depth using the microscope and the micrometer point gage. Two sources of error exist. The zero position was taken with the glass water interface of the channel bottom judged to be at the top of the focal plane. All velocity data were plotted at the center of the focal plane. Since the depth of field of the 50x lens was 11 μ, the actual zero position could have been as much as 3 μ below the assumed value. The 32x lens, which had a depth of field of 24 μ, could produce a 6 μ error. This error would result in a shift of the entire velocity profile, giving the appearance of a positive velocity at the boundary. The other error source was due to the dial reading. The micrometer screw was calibrated using the dial gage and was found to require a correction factor of approximately 0.88 for the lower 200 μ range of movement and a correction factor of 0.95 for movement beyond this range. Since the smallest division on the dial gage was 12.5 μ, the corrected micrometer screw reading was used in the lower 200 μ range. This resulted generally in values 5 - 10 μ above those of the dial gage. In retrospect it appears that the error in locating the position of the focal plane is the largest single error in basic data in the experiment. It is of particular importance since it directly effects the slope of the average velocity profile, and hence the boundary shear computation. Future work will be directed toward reducing this error.

5.2 — Errors in Computed Flow Parameters Due to Data Errors

The "instantaneous" velocity error is due to errors in scale, coordinates, and time. The scale error is negligable but the latter two must be considered.

The velocity is determined by

$$u_i = \frac{\Delta x_i}{\Delta t_i} = \frac{x_{i+1} - x_i}{t_{i+1} - t_i} \tag{9}$$

where u_i = "instantaneous" particle velocity, x_i = coordinate position of the particle in frame i and t_i = time corresponding to frame i. The x_i coordinates were determined as the difference between the point coordinates and the zero coordinates on each frame and thus required a total of four position determinations. If the errors are cumulative, the total maximum absolute error in the distance traveled between frames is

$$E_a(\Delta x_i) = 4E_a(x_i) \tag{10}$$

Since $\Delta t = \frac{10^{-3} \text{ sec/flash}}{\Delta F \text{ frames/flash}}$, the error in time increment Δt_i can be determined from Eq. (8)

$$E_a(\Delta t_i) = 2E_a(t) = .02\ \Delta t_i \tag{11}$$

The maximum absolute error in a velocity measurement is then

$$E_a(u_i) = \frac{E_a(\Delta x_i)}{\Delta t_i} + \frac{\Delta x_i}{(\Delta t_i)^2} E_a(\Delta t_i) \tag{12}$$

Using Eqs. (10) and (11) and the fact that $\Delta x_i = u_i \Delta t_i$

$$E_a(u_i) = \frac{4}{\Delta t_i} E_a(x_i) + 0.02\ u_i \tag{13}$$

The relative error $E_r(u_i)$ is

$$E_r(u_i) = \frac{E_i(u_i)}{u_i} = \frac{4}{u_i \Delta t_i} E_a(x_i) + .02 \qquad (14)$$

An error estimate may be made by consulting the results in Tables 2 and 3. For example, typical data for a particle near the bottom at $y^+ = 0.1$ are $u_i = 0.0245$ ft/sec, $E_a(x_i) = 0.75 \times 10^{-6}$ ft, $\Delta t_i = 0.001$ sec. Substitution in Eq. (14) yields $E_r(u_i) = 12$ percent. For a particle located at $y^+ = 14.2$, $u_i = 0.572$ ft/sec, $E_a(x_i) = 1.7 \times 10^{-6}$ ft, $\Delta t_i = 2 \times 10^{-4}$ sec, which yields $E_r(u_i) = 7.0$ percent.

It should be recognized that the above results are maximum error estimates for a single velocity determination. The average velocity at a given point as computed by Eqs. (1) or (2) is the result of many determinations of u_i. Since the errors are random in sign, the error in the average and instantaneous velocities is less than indicated above.

The error in intensity can be estimated by modifying Eq. (5) to include the error in computing u_j.

$$E_a(\overline{u'^2}) = \frac{1}{n} \sum_1^n [\bar{u} - (u_j + E_a(u_j))]^2 - \overline{u'^2} \qquad (15)$$

Eq. (15) can be expanded and simplified to yield

$$E_a(\overline{u'^2}) = \frac{1}{n} \sum_1^n E_a^2(u_j) - \frac{1}{n} \sum_1^n 2E_a(u_j)(\bar{u} - u_j) \qquad (16)$$

Since $E_a(u_j)$ can be positive or negative, the second term in Eq. (16) will become small as n, the number of particles, increases. The result is

$$E_a\,(\overline{u'^2}) = E_a{}^2(u_j) \tag{17}$$

and

$$E_r\left(\sqrt{\overline{u'^2}}\right) = \frac{E_a(u_j)}{\sqrt{\overline{u'^2}}} \tag{18}$$

Now $E_{a_m}(u_j)$ can be computed from Eq. (13) with u_j replacing u_i and $\Delta t_j = \sum_1 \Delta t_i$ as defined in Eq. (12). Typical data from Table 2 can be used to evaluate Eq. (18). At $y^+ = 0.10$, $u = 0.0245$ ft/sec, $\sqrt{\overline{u'^2}} = 0.0156$ ft/sec and with the camera speed used, a typical particle required 0.0132 sec to travel the length of the observation field. Using $E_{(a)}(x_i) = 10^{-6}$ ft the result is $E_r\left(\sqrt{\overline{u'^2}}\right) = 50$ percent. At $y^+ = 14.2$, $u = 0.572$ ft/sec, and $\sqrt{\overline{u'^2}} = 0.141$ ft/sec a typical particle moved through the observation field much faster so that $\Delta t_j = 1.2 \times 10^{-3}$ sec. The result in this case is $E_r\left(\sqrt{\overline{u'^2}}\right) = 10.5$ percent. It should be recognized that these estimates are high since they assume that the maximum error was made for each velocity determination. Nevertheless, the relative error is always positive, and one could expect the computed intensities to be too high.

5.3 — Computational Errors Due to Depth of Focal Field

There are errors in average velocity and turbulence intensity computation which are due to the fact that particle location cannot be

established within the depth of field and that the average velocity varies within it. Therefore, depending on the computational method, systematic errors can develop which may depend on the distribution of sampled particles within the field and, in fact, increase as the number of particles considered increases.

It has already been pointed out that average velocity computed by Eq. (1) can yield erroneous results. A quantitative estimate of this error can be made. Consider a two-dimensional velocity profile $u = \alpha y$ and assume that the region from y_1 to y_2 corresponds to the field of focus and the distribution of particles in the y direction is uniform.

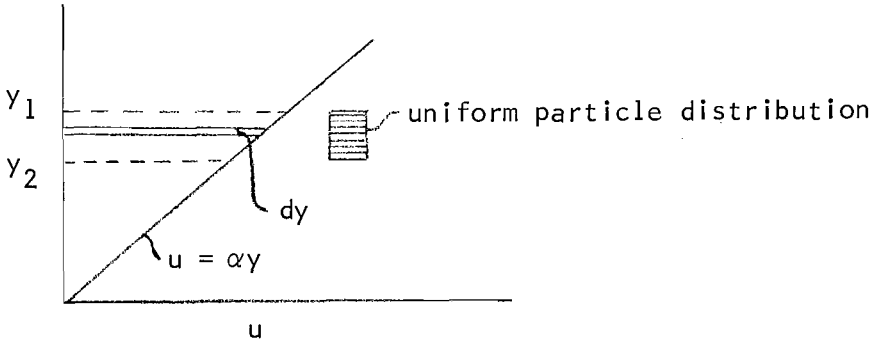

Assume that in each region d_y one particle is followed for a distance Δx and the average velocity in the total region between y_1 and y_2 is calculated according to Eq. (1).

$$\bar{u}_1 = \frac{1}{\sum_{y_1}^{y_2} \Delta t_y} \sum_{y_1}^{y_2} u_y \Delta t_y \tag{19}$$

where Δt_y = time required for a particle at level y to travel a distance Δx and u_y is the velocity at level y.

The numerator of Eq. (1) can be transformed into an integral by recognizing that $\Delta t_y = \frac{\Delta x}{u_y}$ and that a uniform line density of particles, ρ_p, is assumed so that

$$\sum_{y_1}^{y_2} u_y \Delta t_y = \rho_p \int_{y_1}^{y_2} u_y \frac{\Delta x}{u_y} dy = \rho_p \Delta x (y_2 - y_1) \tag{20}$$

Similarly the denominator can be transformed.

$$\sum_{y_1}^{y_2} \Delta t_y = \int_{y_1}^{y_2} \frac{\Delta x}{u_y} \rho_p \, dy = \Delta x \, \rho_p \int_{y_1}^{y_2} \frac{dy}{\alpha y} = \frac{\Delta x \rho_p}{\alpha} \log_e \frac{y_2}{y_1} \tag{21}$$

The result is

$$\bar{u} = \frac{\rho_p \Delta x (y_2 - y_1)}{\frac{\Delta x \rho_p}{\alpha} \log_e \frac{y_2}{y_1}} = \frac{\alpha (y_2 - y_1)}{\log_e \frac{y_2}{y_1}} \tag{22}$$

Since the correct velocity is given by $\bar{u} = \frac{\alpha}{2}(y_2 + y_1)$, the relative error is

$$E_r(\bar{u}) = \frac{1}{\frac{\alpha}{2}(y_2+y_1)} \left[\frac{\alpha}{2}(y_2+y_1) - \frac{\alpha (y_2 - y_1)}{\log_e \frac{y_2}{y_1}}\right] = 1 - \frac{2(y_2 - y_1)}{(y_2+y_1) \log_e \frac{y_2}{y_1}} \tag{23}$$

This result indicates that the method always yields velocities which are too low. For example, consider the 50x lens with a depth of field of 11 μ located near the boundary with $y_1 = 1\ \mu$ and $y_2 = 12\ \mu$. Equation (23)

yields a 32 percent error. However, if $y_1 = 10\ \mu$ and $y_2 = 21\ \mu$ the error is 4 percent. For the 32x lens with a depth of field of 24 μ located at $y_1 = 50\ \mu$, $y_2 = 74\ \mu$ the result is a 2 percent error. It is seen that this error decreases rapidly with distance from the boundary. This error is strong justification for the use of Eq. (3) rather than Eq. (1).

The above discussion indicates that Eq. (3) would yield the correct average velocity if a uniform particle sampling across the depth of field is made. However, this is not true in the computation of the turbulence intensity using Eq. (5) which is analogous to Eq. (3) in that each particle is given the same weight in the computation. Consider the same two-dimensional velocity profile just discussed with a uniform particle sampling throughout the region y_1 to y_2. Equation (5) can be transformed into integral form assuming a uniform sample distribution from y_1 to y_2.

$$\overline{u'^2} = \frac{1}{y_2-y_1} \int_{y_1}^{y_2} (\bar{u}-u_j)^2 \, dy \tag{24}$$

By substituting $u_j = \alpha_y$, $\bar{u} = \frac{\alpha}{2}(y_1+y_2)$ and integrating, the result is

$$\sqrt{\overline{u'^2}} = \frac{\alpha}{\sqrt{12}} (y_2-y_1) \tag{25}$$

By dividing by the local average velocity and the shear velocity, two relative intensities are obtained.

$$\frac{\sqrt{\overline{u'^2}}}{\bar{u}} = \frac{y_2 - y_1}{\sqrt{3}(y_2 + y_1)} \tag{26}$$

$$\frac{\sqrt{\overline{u'^2}}}{u_\tau} = \sqrt{\frac{\alpha}{12\nu}}\,(y_2 - y_1) \tag{27}$$

Equations (25), (26), and (27) indicate that because a velocity gradient exists across the depth of field, Eq. (5) may yield a positive result even if no turbulent velocity fluctuations exist. Recognizing that $\alpha = \frac{\tau_o}{\mu}$, and since $(y_2 - y_1)$ is the depth of field, Eqs. (25) and (27) can be evaluated for each lens. The result is an apparent intensity of 0.0046 ft/sec and a relative intensity using the shear velocity of 0.077 for the 50x lens and 0.010 ft/sec and 0.17 respectively for the 32x lens. Eq. (26) yields an apparent relative intensity which depends on the distance from the boundary. The cross correlation, $\sqrt{\overline{u'w'}}$ does not contain an inherent error since no average velocity gradient in the w direction exists at the center of the channel.

It should be emphasized that the preceeding apparent errors were computed assuming a uniform particle sampling across the depth of field. It is not likely that this is true because of the relatively few number of particles sampled.

5.4 — Error Due to Relative Particle Velocity

The assumption that the particles have zero velocity relative to the fluid surrounding them is basic to the experimental work. This

assumption is obviously not completely true, and it is of interest to estimate the degree to which the particle motion differs from that of the fluid.

First, the particles have a settling velocity which can be computed from Stokes' law assuming the particle Reynolds' number, ud/ν, is less than unity. Where U = settling velocity, d = particle diameter and ν = kinematic viscosity, the result is

$$U = \frac{2}{9}\frac{d_2}{\mu}(\gamma_p - \gamma) \tag{28}$$

where μ = viscosity, γ_p = specific weight of the particle and γ = specific weight of water. Using typical experimental values, d = 1 μ = 3.28 x 10^{-6} ft, μ = 1.94 x 10^{-5} lb sec/ft^2, and γ_p = 1.05, the settling velocity is U = 0.9 x 10^{-7} ft/sec with a Reynolds' number = 3 x 10^{-8}. Assuming a typical particle is followed for a period of 10^{-3} sec the total fall distance is about 3 x 10^{-5} μ which is much less than 11 μ, the depth of field of the microscope lens. Therefore, the settling velocity is negligible.

In addition to the fall velocity, the particles have a lift force exerted on them due to rotation and their presence in a velocity gradient field. Although considerable work has been done on this problem for an ideal fluid, the viscous case still bears study. Reference is made here to the experimental work reported by Small[19]. The result of interest is an expression for a lift coefficient, C_L, which presumably embodies the net effect of rotation and shear field. The empirical equation which describes the data is

$$C_L = 7 \times 10^{-4} \left[\left(\frac{d}{u}\frac{du}{dy}\right)\left(\frac{d}{D}\right)\left(\frac{1}{N_{R_p}}\right)\right]^2 \qquad (29)$$

where d = particle diamter, u = local fluid velocity, $\frac{du}{dy}$ = local velocity gradient, D = pipe diameter and $N_{R_p} = \frac{ud}{\nu}$. This can be evaluated using data from this report: d = 1 μ = 3.28×10^{-6} ft, u = 1 ft/sec, $\frac{du}{dy} = \frac{\tau_o}{\mu} = 4.4 \times 10^{-3}$ sec^{-1}, D = equivalent pipe diameter = 4x depth = .16 ft and N_{R_p} = 0.33. The result is $C_L = 5.7 \times 10^{-8}$. The lift force, F_L, can now be computed.

$$F_L = C_L \rho \frac{u^2}{2} \pi \frac{d^2}{4} \qquad (30)$$

The result is $F_L = 4.65 \times 10^{-19}$ lbs. This force can be compared to the submerged weight of the particle assuming a specific gravity of 1.05. The weight is 565×10^{-19} lbs or about 100 times greater than the lift. Thus, the net vertical motion of the particle due to its weight and the lift force toward the channel bottom is negligible.

The response of a particle to a change in the fluid velocity is also an important consideration. Consider a particle released from rest in a fluid moving with velocity u. The equation of motion of the particle can be obtained using Stokes' law. The result is

$$3\mu\pi d(u-u_p) = m\frac{du_p}{dt} \qquad (31)$$

where u_p = particle velocity at time t, m = particle mass and the other symbols as defined previously. Eq. (31) can be integrated between the

limits $o \rightarrow t$ and $o \rightarrow \alpha u_p$ where α is some fraction of u. The result is

$$t = \frac{\rho_p d^2}{18\,\mu} \log_e \frac{1}{(1-\alpha)} \tag{32}$$

where ρ_p = density of the particle. For $\alpha = 0.999$, Eq. (32) yields $t = 4 \times 10^{-7}$ sec. Since the smallest time interval used in the velocity computations was of the order of 10^{-4} sec, it is seen that particle response to fluid acceleration is essentially instantaneous.

The conclusion is that because of the small size and specific gravity of 1.05, the particles act as valid tracers and there is no measurable error associated with this assumption.

6. RESULTS

6.1 — Boundary Shear Stress - Laminar Flow

Boundary shear was experimentally determined for the eight laminar tests and the one turbulent flow test. The Reynolds' number based on the depth for the laminar tests varied from about 3 to 12 while its value for the turbulent test was 4,550. The latter Reynolds' number was the highest that could be achieved since the depth was limited to approximately 0.5 in. by the illumination system. Although a higher N_R is desirable for quantitative purposes, the value achieved is sufficient for purposes of this report.

The boundary shear stress, τ_o, was calculated by plotting the velocity profile in the 100 μ - 200 μ region adjacent to the boundary, computing the slope or the rate of shear and multiplying by the viscosity. The results of these computations are compared with τ_o computed from a two-dimensional static balance in Table 1. It is noted that with the exception of test 7-L, the values agree to within $\pm$ 15 percent. In seven of the nine tests the computed value was higher than the experimental value.

In order to evaluate these results the velocity profiles must be examined. Figures 6 - 13 show the laminar profiles. Each point represents the average velocity of a particle over the width of the field of view. The solid line was arbitrarily drawn through the points and its slope computed. There are three sources of error for any point. The location of the bottom, y = 0, could be as much as 3 - 5 μ lower than

indicated. This would result in an apparent shift of the entire curve indicating an apparent positive velocity at the bottom. All of the velocity determinations at any level were plotted at the center of the focal field, although they could actually occur anywhere within the field which is indicated by the dashed lines on each graph. Thus, any value falling within this region defined by the dashed lines is within the known range of error. Finally, the experimental error in velocity determination is shown by horizontal error flags for an arbitrary particle near the bottom and one farther up in the flow. This error is the result of errors in measurement of time and distance and thus varies with distance from the boundary. It is seen that these errors can account for most of the apparent irregularities in individual points. Thus, a line drawn through the points would not necessarily pass through the origin. This would indicate an error in the initial reference level. The significant aspect of the line is its slope or the shear rate. The variation of shear rate due to the depth of field error can be computed from

$$\frac{du}{dy} = \frac{u_y \mp 5.5\left(\frac{du}{dy}\right)_o}{y \mp 5.5} \tag{33}$$

where y is the largest depth in microns (μ) in the region where the velocity profile is essentially linear, u_y is the velocity at y in μ/sec, $\left(\frac{du}{dy}\right)_o$ is the shear rate estimated by a straight line through the data passing through the origin, and 5.5 μ is one-half the depth of field. This equation reflects only variations resulting from uncertainty in particle location within the depth of field. Application of Eq. (33) to test 1-L,

for example, yields a possible +15 to -9 percent variation in du/dy which compares well with the percent difference in boundary shear shown in Table 1. All of the differences shown in Table 1 may be accounted for by Eq. (33) with the exceptions of test 7-L and the turbulent test which will be discussed later.

Some general aspects of the laminar flow data should be mentioned. Steady, uniform laminar flow in an open channel is very difficult to achieve experimentally because of the small channel slopes required. Figures 10 and 12 indicate such an unsteady condition. This is probably the cause of the large disagreement between the computed and experimental values of τ_o for test 7-L. The photographs were taken initially near the bottom and then progressively higher in the flow. This created a time lag between data points and produced a distorted profile if the flow was unsteady. Because the velocities throughout the flow were relatively low, the entire velocity profile was measured. The results are shown in dimensionless form in Figs. 14 and 15. Figure 14 shows the lower region, essentially the same data as in Figs. 6 - 13, and Fig. 15 shows the entire profile. The line is the theoretical parabolic profile. The scatter near the surface is due to error in velocity determination since the depth of field error is insignificant at large distances from the bottom.

6.2 — Boundary Shear Stress - Turbulent Flow

The velocity data in the sublayer for the turbulent test is shown in Fig. 16. The data points are the average values for each film

computed from Eq. (3). The results from Eq. (1) were not plotted because of the inherent error described by Eq. (23). Both values are listed in Tables 2 and 3 for comparison. The data in the columns headed "By Frame" were calculated from Eqs. (1), (4), and (6) and those under "By Particle" from Eqs. (3), (5), and (7). The vertical error flags in Figs. 16 indicate the depth of field. No horizontal or velocity error flag is shown because each point is the average of from 28 to 141 individual determinations and the resulting error is difficult to establish. As indicated in Chapter 4, the error in an individual determination is approximately $\pm$ 17 percent near the bottom and $\pm$ 7 percent at the top of the sublayer. However, since this is a maximum estimate and it is random, the error in the average would be much less. The statistical error due to sampling might be considered. The difference between the mean of a sample and its population can be estimated within various confidence limits using the "students" t distribution. This method assumes a nearly normal distribution of the population. In this case the population consists of all possible velocity values within the depth of field and thus has a rectangular distribution with depth. However, if the method is used anyway the result of a 95 percent confidence interval is a possible difference between the true and sample means of .375 σ for a sample of 30 and .17 σ for a sample of 140. Since σ, the standard deviation or turbulence intensity, was almost equal to the average velocity near the bottom, as seen in Tables 2 and 3, this would result in a difference of $\pm$ 37.5% for the sample of 30. On the other hand, at the top of the sublayer the standard deviation is about 20 percent of the average velocity which would reduce the possible difference to $\pm$ 7 percent for a sample of 30. It is concluded that the average velocity points near the bottom are subject to a higher level of statistical error than those near the top of the sublayer.

Taking into account the preceding discussion, the line in Fig. 16 was constructed. The points near the bottom were not weighted as heavily as the remainder. It is noted that with the exception of the lowest points, adjustment of the points within the depth could move the points very close or on the line. Also the boundary shear computed from the slope is 12 percent below the value computed from a force balance. This difference is of the same order as for the laminar flow tests. Application of Eq. (33) yields a possible variation of $\pm$ 9 percent. This indicates that the primary source of error in the computation of boundary shear is due to the depth of field of the lens rather than experimental or statistical errors. Fewer samples are required in the laminar flow tests since the flow supposedly contains no random component. The turbulent data requires many more samples to obtain a reasonably valid average velocity. In both types of flow the depth of field uncertainty was the same. It is concluded that an accuracy of approximately $\pm$ 15 percent can be expected for boundary shear computation if the present optical system is used. If a flow system were studied where the ratio of the sublayer thickness to the depth of field is larger the accuracy would be improved provided a large enough particle sample is used for each average velocity computation.

Figure 17 shows the velocity data for the turbulent test plotted using the conventional dimensionless terms y^+ and u^+. The dimensionless depth of field is shown to scale. The value of τ_o used in the computation of u_τ was determined from the equation $\tau_o = \gamma DS$ rather than from the slope of the data of Fig. 16. Reasonable agreement with the "law of the wall", $y^+ = u^+$, is seen. The two points at $y^+ = 11.7$ and 14.2 are presumably in

the transition region between the "law of the Wall" region and the logarithmic region. The dashed line represents the data taken by Runstadler[14] and is presented for qualititative comparison.

It is interesting to compare the values of $\bar{u}_1$ and $\bar{u}_2$ in Tables 2 and 3. As indicated by Eq. (23), $\bar{u}_1$ would be expected to be lower than $\bar{u}_2$, and this is in fact the case for each film. Furthermore, the percentage differences between $\bar{u}_1$ and $\bar{u}_2$ decrease with distance from the bottom as predicted by Eq. (23). In Table 1 the difference between $\bar{u}_1$ and $\bar{u}_2$ varies from a maximum of 24 percent at $y^+ = 0.10$ to 2.5 percent at $y^+ = 4.15$ and in Table 2 the variation is from 50 percent to 5 percent. Equation (23) yields a difference of 37 percent for the top and bottom of the focal field at 9.0 μ and 0.5 μ from the bottom respectively, which agrees reasonable well with the observed differences. However, the predicted difference decreases very rapidly with increasing distance from bottom, being about 1 percent for $y^+ = 1.0$ for the 50x films and 2.68 for the 32x films. The observed differences at these levels, for example, are 10.2 and 8.0 percent, higher than predicted values. Since Eq. (23) assumes a uniform particle sampling, the departure of the observed differences indicates that perhaps more particles were sampled from the lower than from the upper part of the focal field.

6.3 — Turbulence Intensity

The results of the rms of the velocity fluctuations as computed by Eqs. (4) and (5) are shown in Tables 2 and 3. As described in Section 5.3, the computed logitudinal intensity, $\sqrt{\overline{u_2'^2}}$, should be regarded as an apparent value since it contains a component due to the variation in mean

velocity across the depth of field. This component is estimated by Eq. (25) and in terms of relative intensity by Eqs. (26) and (27). The apparent intensity as computed by Eq. (4), $\sqrt{\overline{u_1'^2}}$, contains additional error due to the error in computation of $\bar{u}_1$, therefore these results are not presented graphically but are listed in the Tables 2 and 3 for comparison.

A plot of Eq. (26) for both lenses is shown in Fig. 18. It is seen that the error in relative intensity increases rapidly, reaching a maximum of $1/\sqrt{3}$ when the lower edge of the focal plane coincides with the boundary.

The computed relative intensities based on the local average velocity are plotted in Fig. 19. The hollow symbols are these values corrected using Eq. (26). The data clearly indicates the presence of an error similar to that predicted by Eq. (26). The maximum relative intensity at the wall estimated by Hanratty[17], for example, is 0.32. This compares favorably with the corrected data with the exception of two points.

The lateral relative intensity, $\sqrt{\overline{w_2'^2}}/\bar{u}_2$, is shown in Fig. 20. Since there is no average velocity gradient in the w direction the values do not contain an apparent intensity component. The plot indicates a rise in relative intensity as the wall is approached. The line shown was derived from a combination of two graphs presented in Laufer's report.[12]

Plots of the relative intensity based on the shear velocity in the u and w directions are shown in Figs. 21 and 22 respectively. The data of Fig. 21 is uncorrected. The corrections based on Eq. (27) are shown to scale by the arrows. Results reported by Rundtadler[14], Bakewell[16] and Laufer[12] are shown for comparison.

One disadvantage of the experimental method is the short time length of each film. This was necessary since the high-speed camera had a capacity of only 100 ft of film. The time length was marginal for computation of intensity and much too short for any attempt at autocorrelation computations. Improvement might be made by sampling more particles, but there is danger in sampling two particles simultaneously since they may be following the same eddy and therefore consideration of both would improperly influence the average velocity and intensity.

The compution of intensity by individual frames using Eq. (4) has the potential advantage of including higher frequency fluctuations than computation by particle. For example, the lowest film speed used was approximately 1000 frames/sec which means that analysis by frame could include frequencies up to 1000 sec^{-1} while if the particle were followed for 5 frames the highest frequency which could be measured is 200 sec^{-1}. This is not expected to be a major problem in sublayer turbulence measurements in water since most of the energy is associated with frequencies below 100 sec^{-1}.

6.4 — Distribution of Particle Velocities

The distributions of the longitudinal particle velocities for each film were plotted in the form of histograms with an interval of $0.2\sqrt{\overline{u_2'^2}}$. Four examples are shown in Fig. 23. In addition the data of films 1-A, 2-A, and 1-B, and 3-A, 4-A, and 2-B were combined into two histograms shown in Fig. 24. This combination gives a more meaningful distribution because of the large sample size. The third moment or skewness of the histograms about the mean velocity was computed for each

film and the two combined sets. The results are tabulated in Tables 2 and 3 and plotted in Fig. 25.

The significant aspect of these computations is that all of the distributions with the exception of film 3-A exhibited a positive skewness. This agrees qualitatively with the data reported by Comte-Bellot[20] shown in Fig. 25.

It must be recognized that the distribution and the resulting skewness are a result of a combination of two factors, the character of the turbulence and the uncertainty of the location of a particle within the depth of field. Thus, a particle with a velocity above the mean could be located near the top of the focal field or in a high velocity eddy. However, the consistant positive skewness indicates that this is a characteristic of the flow, but the relatively low number of particles sampled in each distribution makes quantitative deduction highly questionable.

6.5 — Evaluation of the Method

The principal advantages of the method are that the flow is not disturbed, calibration is simple, and the flow in a very small region is observed. There are two main disadvantages. First, the time and effort required to analyze the films is almost prohibitive under the procedure employed. Also, the short length of record and the uncertainty due to a finite depth of focal field result in uncertainties in turbulence computations which increase as the boundary is approached, this being the area of primary interest. The thickness of the sublayer region could be increased in relation to the depth of field, but this may not be practical.

It has been shown that the procedure of computing the velocity for each frame yields erronious results and is also very time consuming. A more proper method would be to record the motion of all particles over the same number of frames while still observing only one particle at a time.

A modification of the method reported by Chen[9] and Elrick[10] is proposed as the next phase of the current work. This method views the particle motion in a plane normal to the boundary. The particle and its reflected image are recorded on the film, thus permitting precise location of the boundary and eliminating the problems associated with the large velocity gradient across the depth of field. Velocity profiles normal to the vertical walls of an open channel will be studied. This will permit the determination of the distribution of boundary shear along the vertical wall along with turbulence characteristics in the u and v direction.

Table 1. Boundary Shear Data

$$u_{max}\ (calc.) = \frac{gSD^2}{2\nu}$$

Test No.	Depth μ	Slope	N_R	ν ft^2/sec	Max Velocity μ/sec		Boundary Shear $\tau_o = \gamma DS$	Boundary Shear $\tau_o = \mu \frac{du}{dy}$	Percent Diff
					Exp.	Calc.			
1-L	788	0.0015	3.7	0.94×10^{-5}	6,100	5,260	24.1×10^{-5}	26.2×10^{-5}	+8.7
2-L	2,240	0.00020	7.2	1.00	4,600	5,270	9.16	8.05	-12.1
3-L	2,340	0.000192	7.5	1.00	4,540	5,490	9.18	7.90	-14.0
4-L	2,630	0.00016	10.6	0.86	5,520	6,670	8.60	7.42	-13.8
5-L	2,540	0.00016	12.0	0.86	5,750	6,320	8.28	7.98	- 3.6
6-L	2,590	0.00014	11.3	0.86	5,430	5,750	7.40	7.70	+ 4.0
7-L	2,340	0.000175	10.3	0.88	5,516	5,770	8.34	5.07	-39.3
8-L	2,340	0.000195	10.5	0.92	5,892	7,730	9.32	10.6	-13.7
Turb.	12,420	0.00353	4,550	0.895	—	—	845.	745.	-12.0

Table 2. Turbulent Flow Results — 50x Lens

D = 0.489 in. S = .00332 u_τ = 0.0664 ft/sec

U = Q/A = 1.00 ft/sec $\nu = 0.895 \times 10^{-5}$ ft^2/sec

					By Frame					By Particle					
Film	y(μ)	y+	No. Part.	Time (sec)	$\bar{u}_1$ ft/sec	$\bar{w}_1$ ft/sec	$\sqrt{\overline{u_1'^2}}$ ft/sec	$\sqrt{\overline{w_1'^2}}$ ft/sec	$\overline{u'w'}_1$ (x10^5)	$\bar{u}_2$ ft/sec	$\bar{w}_2$ ft/sec	$\sqrt{\overline{u_2'^2}}$ ft/sec	$\sqrt{\overline{w_2'^2}}$ ft/sec	$\overline{u'w'}_2$ (x10^5)	$\frac{\overline{u_2'^3}}{(\overline{u_2'^2})^{3/2}}$
1A	4.5	0.10	85	2.20	0.0187	0.00007	0.0123	0.0056	-0.62	0.0245	-0.00078	0.0156	0.0068	-2.10	0.283
2A	4.5	0.10	60	2.08	0.0283	0.00034	0.0132	0.0062	-0.124	0.0331	-0.00056	0.0162	0.0064	0.737	0.271
3A	41	1.00	63	2.28	0.0557	0.00448	0.0194	0.0129	0.606	0.0621	0.0057	0.0159	0.0113	4.57	-0.094
4A	41	1.00	118	2.12	0.0610	0.0018	0.0281	0.0141	3.96	0.0751	0.0045	0.0352	0.0235	30.7	0.418
5A	88	2.14	28	1.28	0.131	0.0073	0.0531	0.0224	-0.02	0.147	0.0081	0.582	0.0221	-2.38	0.823
6A	123	3.00	63	0.88	0.187	0.0012	0.0450	0.0442	2.98	0.195	-0.0005	0.0452	0.0259	3.82	0.658
7A	123	3.00	39	0.88	0.176	-0.0113	0.0540	0.0340	1.89	0.195	-0.0136	0.0542	0.0392	-2.06	0.089
8A	170	4.15	54	0.717	0.228	0.0043	0.0559	0.0344	1.41	0.234	0.0061	0.0560	0.0348	9.39	0.701

Table 3. Turbulent Flow Results — 32x Lens

$D = 0.489$ in. $\quad U = Q/A = 0.995$ ft/sec $\quad S = .00332$

$\nu = 0.875 \times 10^{-5}$ ft^2/sec $\quad u_\tau = 0.0664$ ft/sec

					By Frame					By Particle					
Film	y(μ)	y+	No. Part.	Time (sec)	$\bar{u}_1$ ft/sec	$\bar{w}_1$ ft/sec	$\sqrt{\overline{u_1'^2}}$ ft/sec	$\sqrt{\overline{w_1'^2}}$ ft/sec	$\overline{u'w'}_1$ (x10^5)	$\bar{u}_2$ ft/sec	$\bar{w}_2$ ft/sec	$\sqrt{\overline{u_2'^2}}$ ft/sec	$\sqrt{\overline{w_2'^2}}$ ft/sec	$\overline{u'w'}_2$ (x10^5)	$\frac{\overline{u_2'^3}}{(\overline{u_2'^2})^{3/2}}$
1B	4.5	0.11	63	2.18	0.0176	-0.0009	0.0195	0.0125	2.69	0.0356	-0.0022	0.0188	0.0085	-2.66	0.502
2B	34	0.85	141	2.33	0.0571	-0.0015	0.0227	0.0113	-1.22	0.0640	-0.0022	0.0248	0.0112	0.686	0.651
3B	34	0.85	31	1.79	0.0620	-0.0002	0.0179	0.0115	-2.07	0.0672	-0.0020	0.0176	0.0111	-5.31	0.304
4B	107	2.68	48	0.79	0.1234	0.0056	0.0366	0.0232	-1.68	0.1344	0.0048	0.0427	0.0226	8.40	1.469
5B	164	4.10	31	0.94	0.220	0.0136	0.0576	0.0336	-0.38	0.232	0.0085	0.0652	0.0340	-7.17	0.087
6B	468	11.7	43	0.74	0.517	0.0006	0.156	0.0582	-13.1	0.518	-0.0021	0.163	0.0594	-476.	0.824
7B	568	14.2	53	0.70	0.542	0.0101	0.140	0.0686	-8.05	0.572	0.0064	0.141	0.0669	-198.	0.520

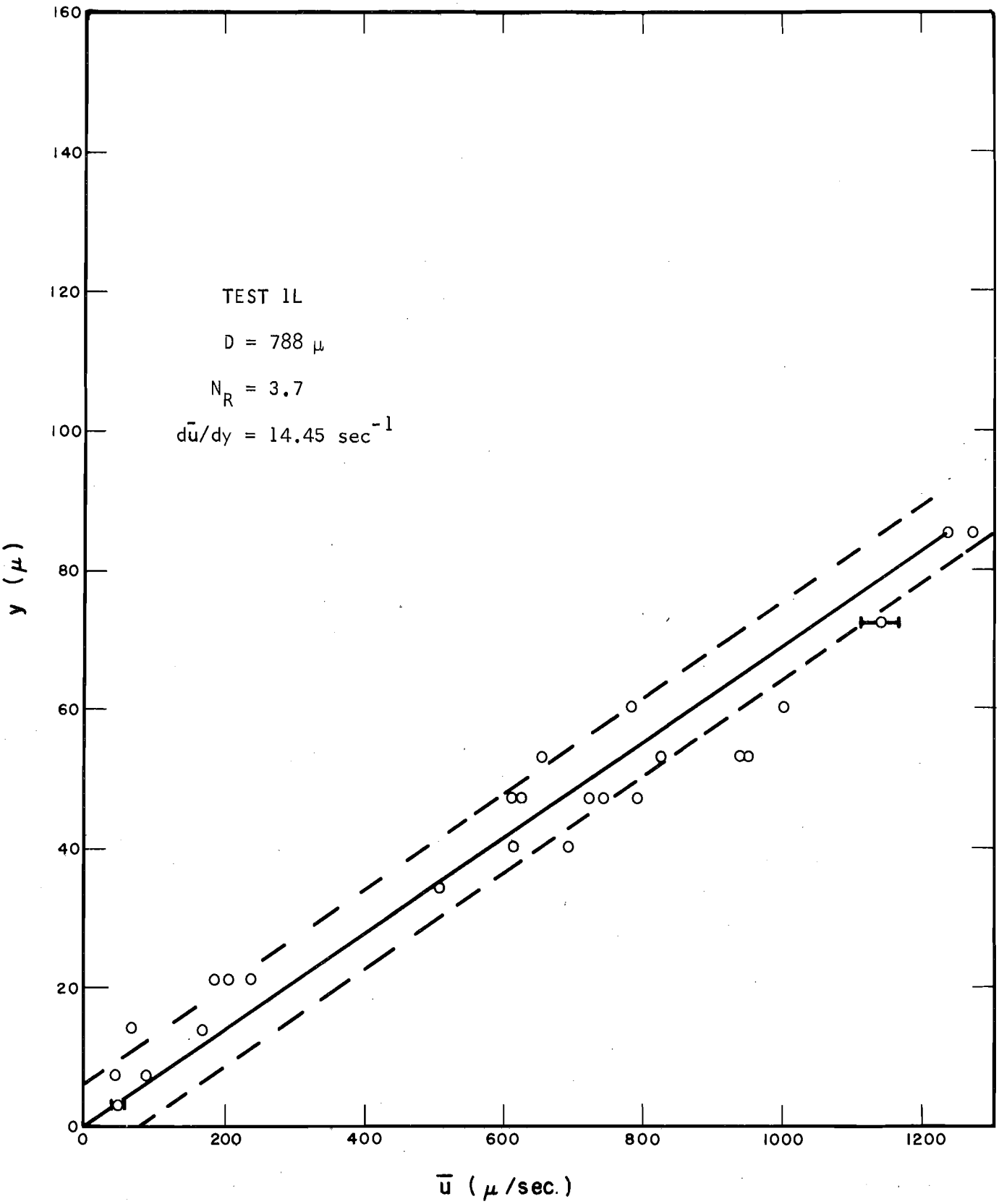

Fig. 6 — Laminar Velocity Profile

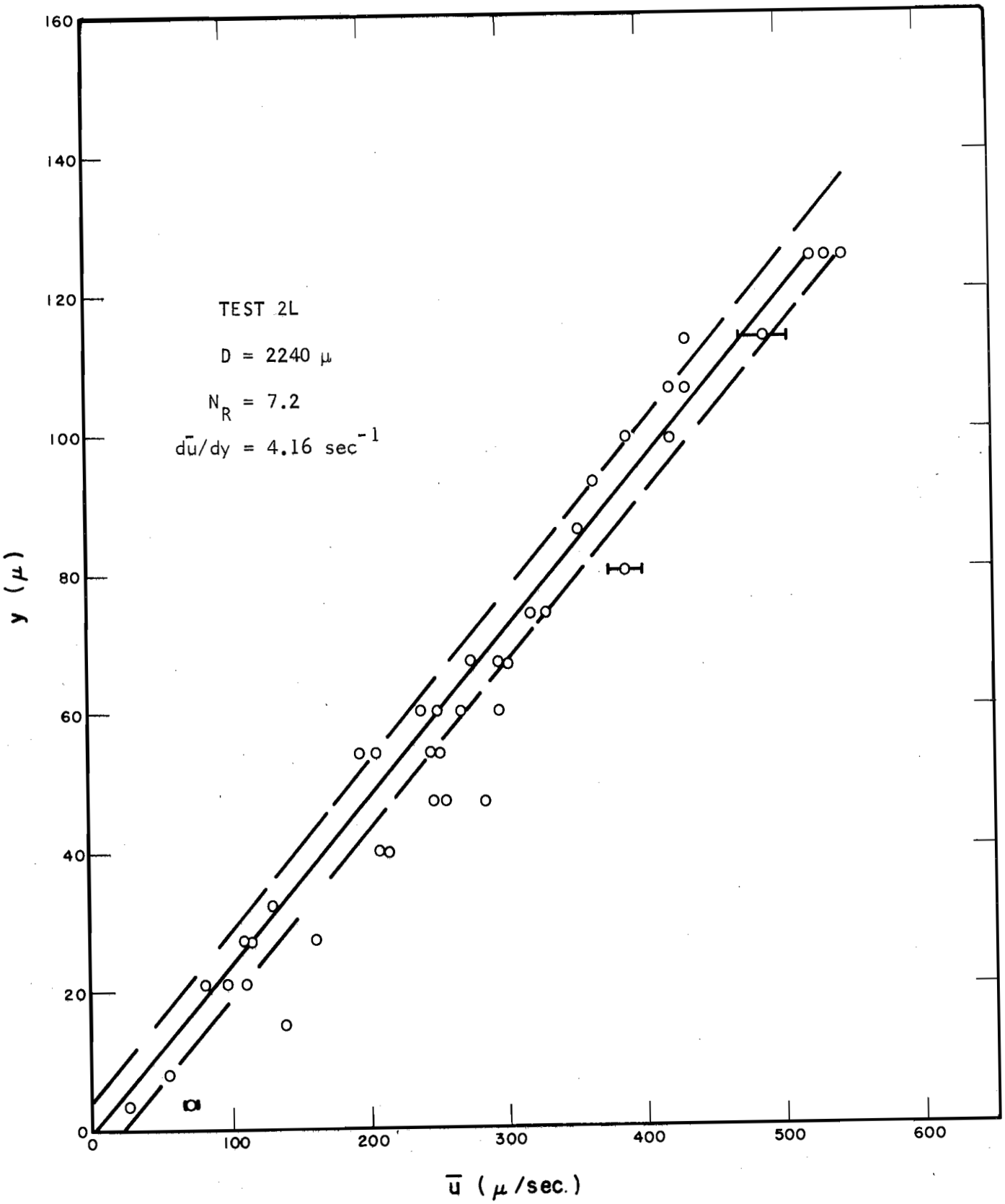

Fig. 7 — Laminar Velocity Profile

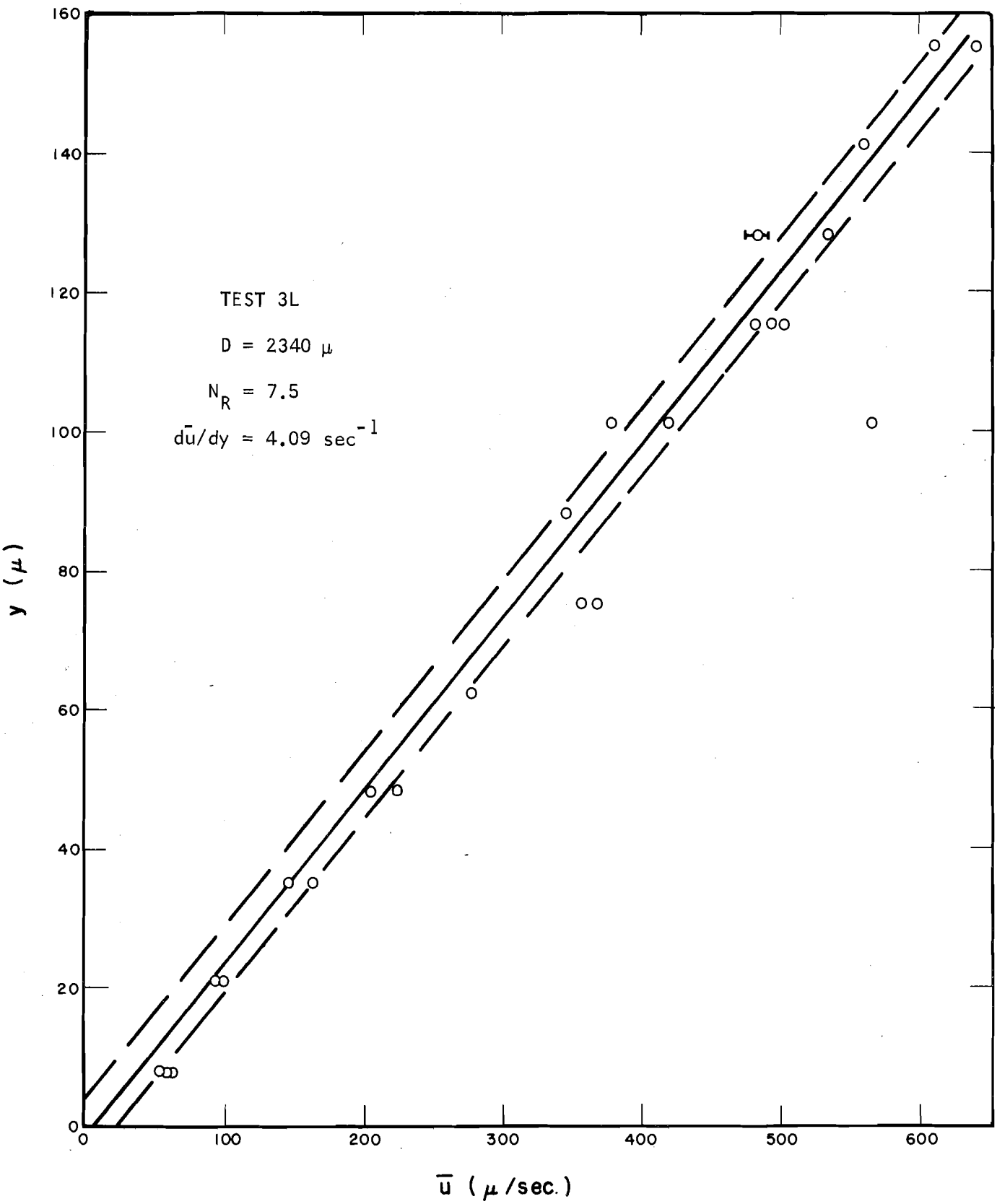

Fig. 8 — Laminar Velocity Profile

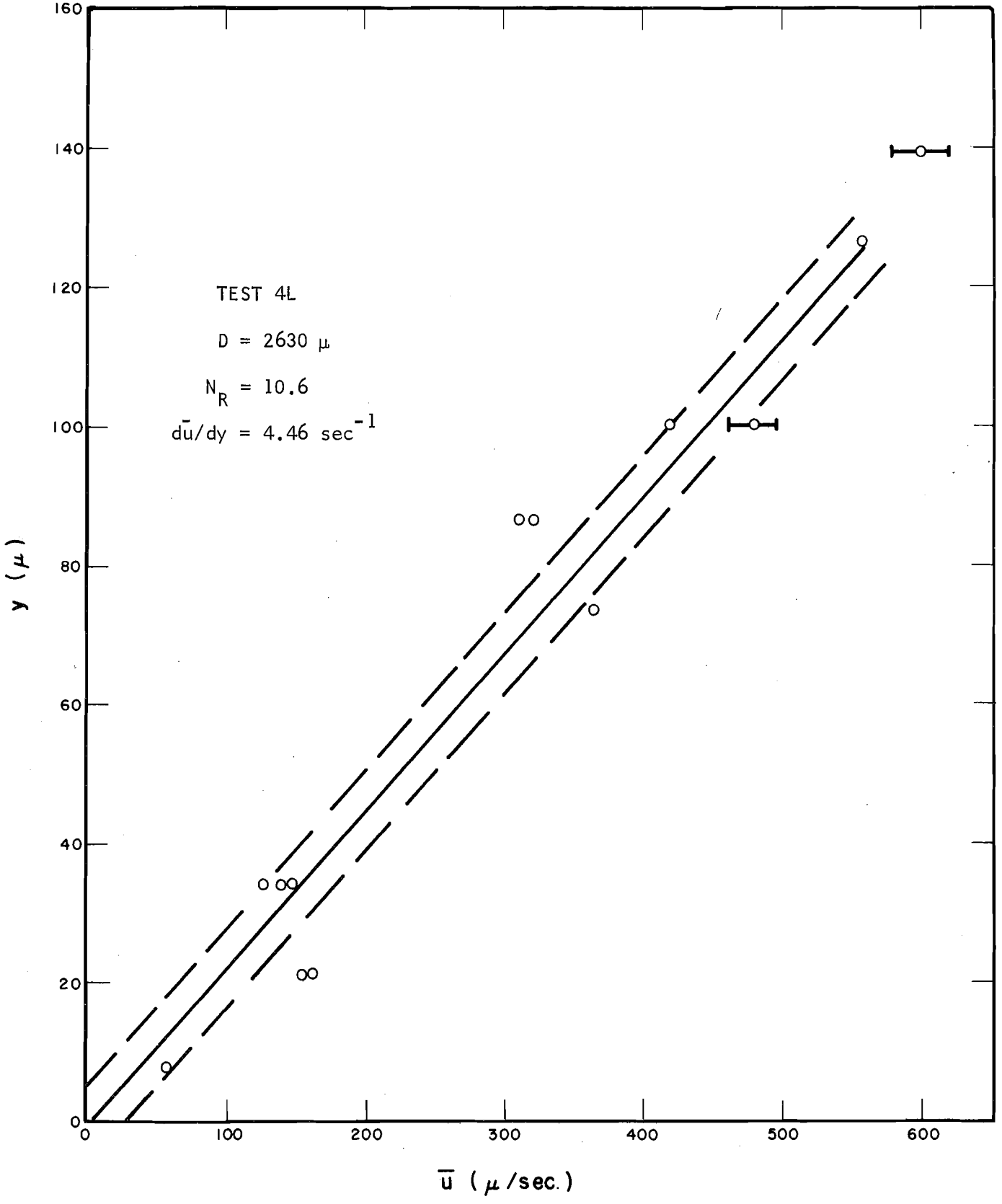

Fig. 9 — Laminar Velocity Profile

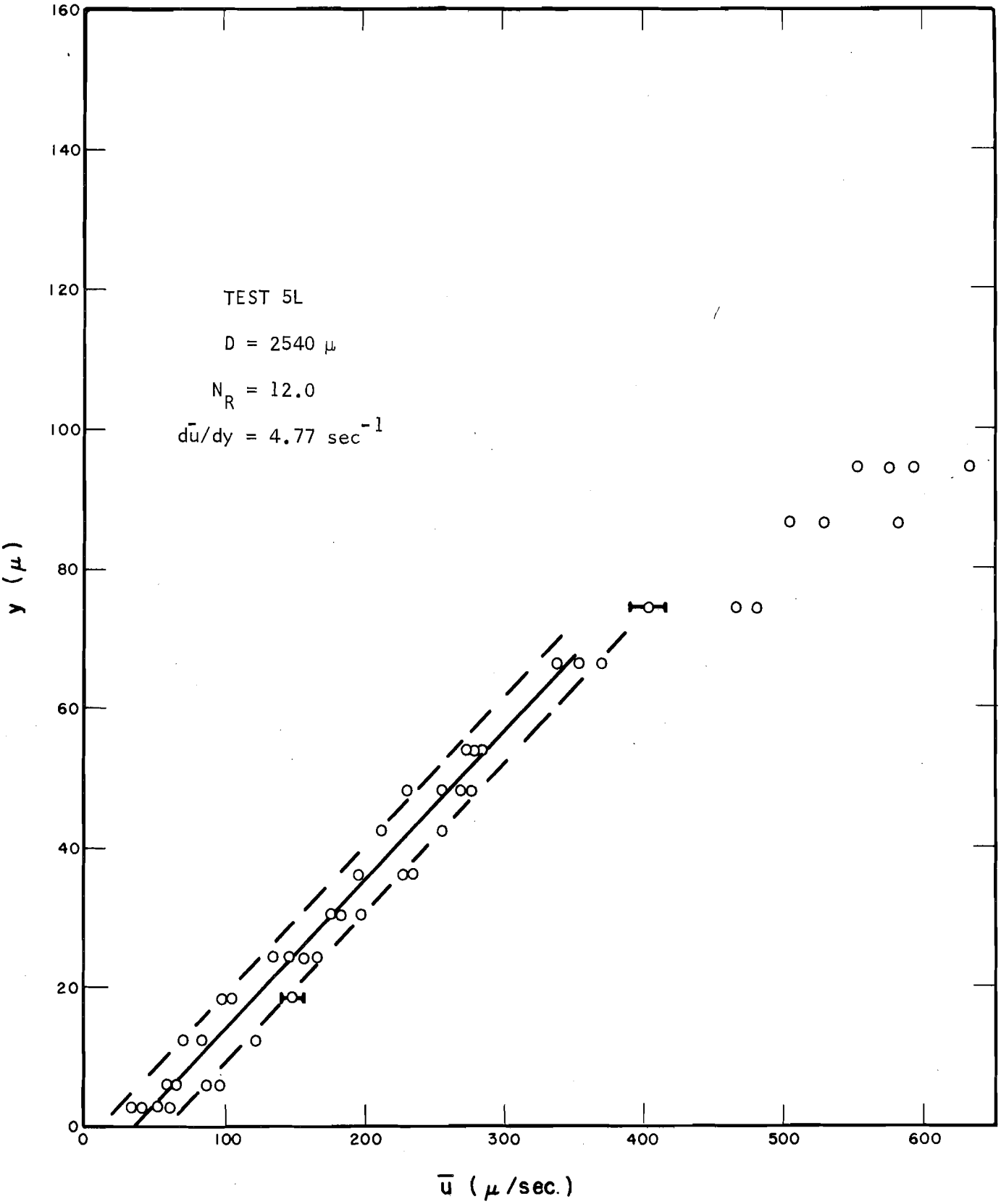

Fig. 10 — Laminar Velocity Profile

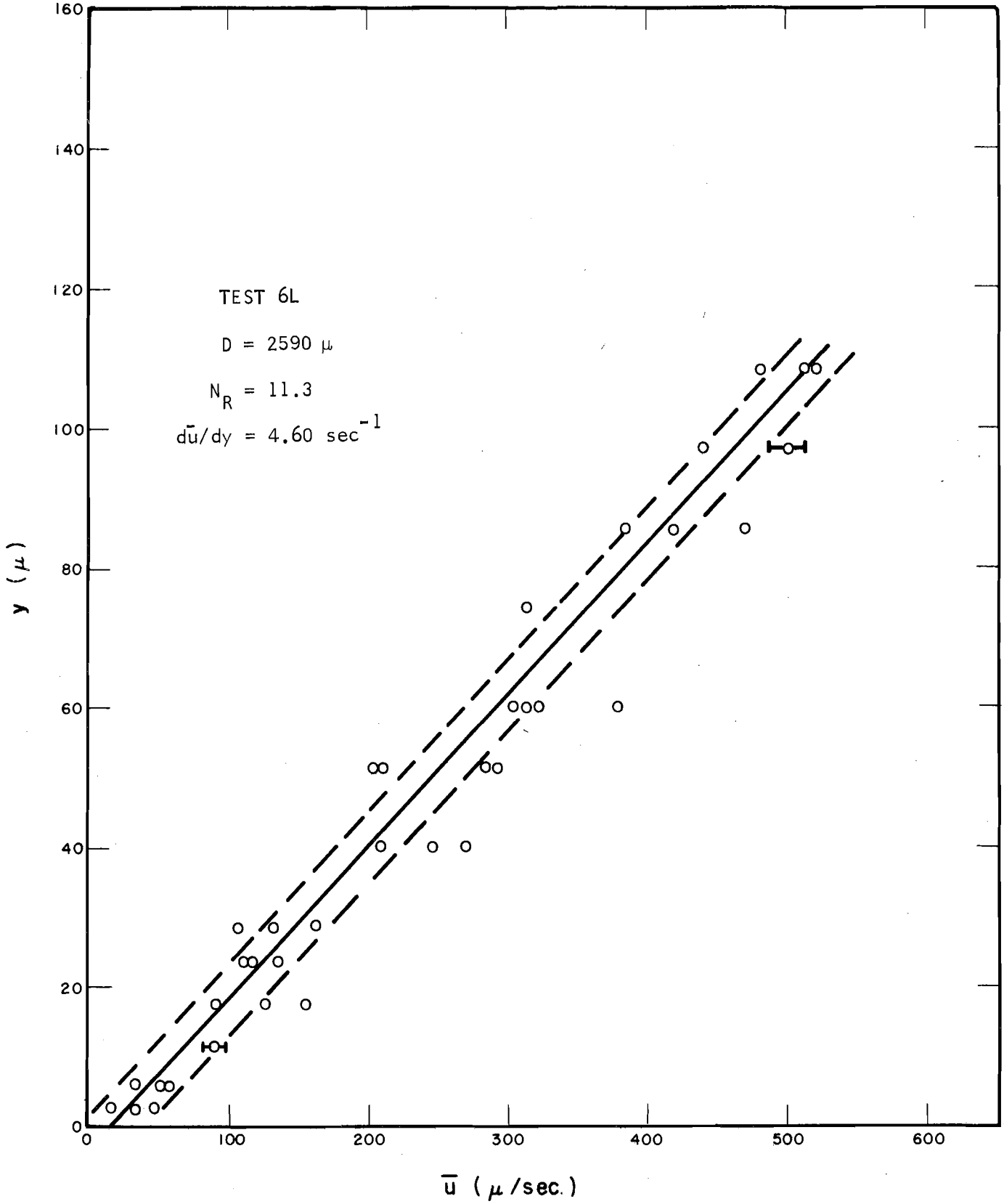

Fig. 11 — Laminar Velocity Profile

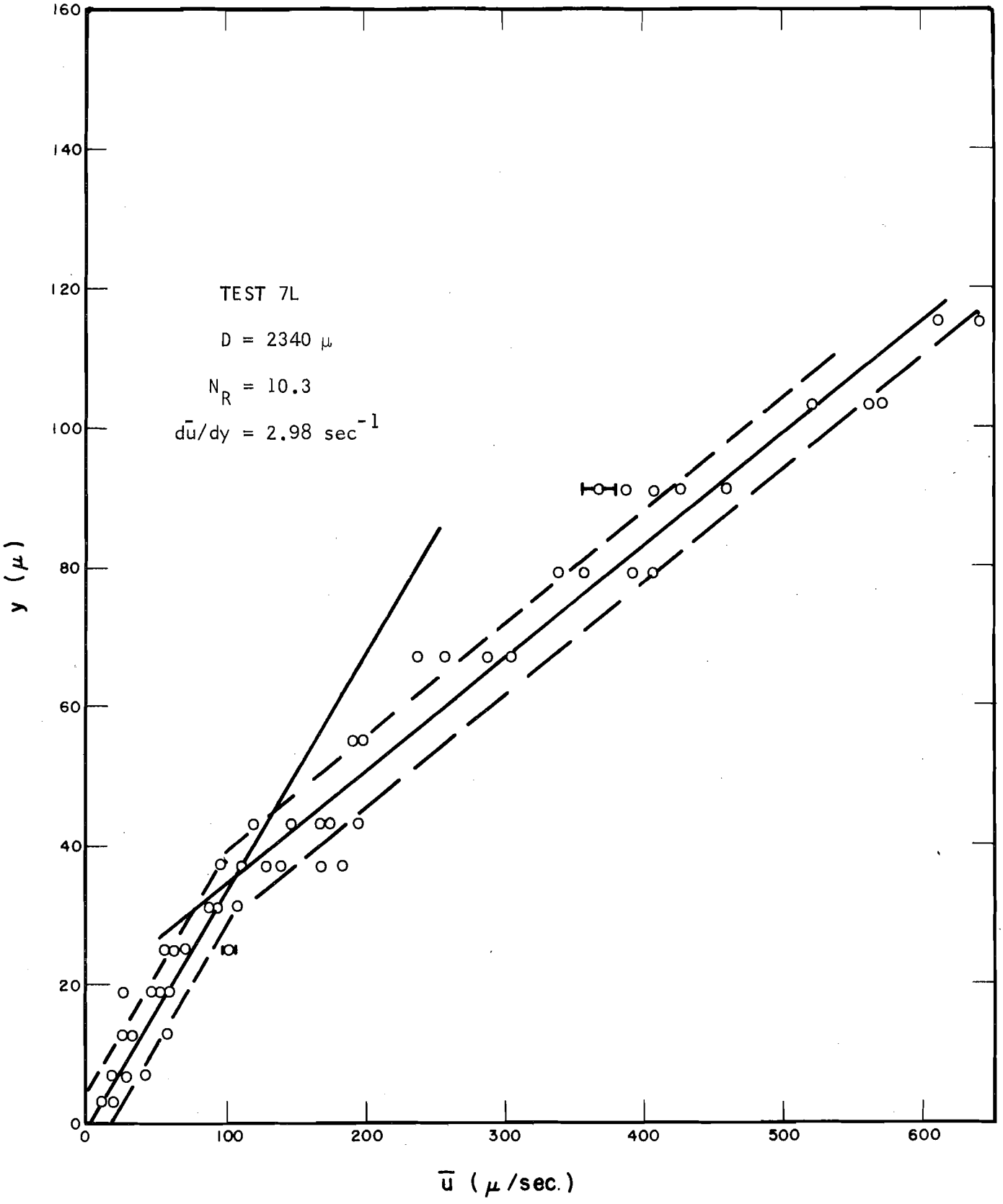

Fig. 12 — Laminar Velocity Profile

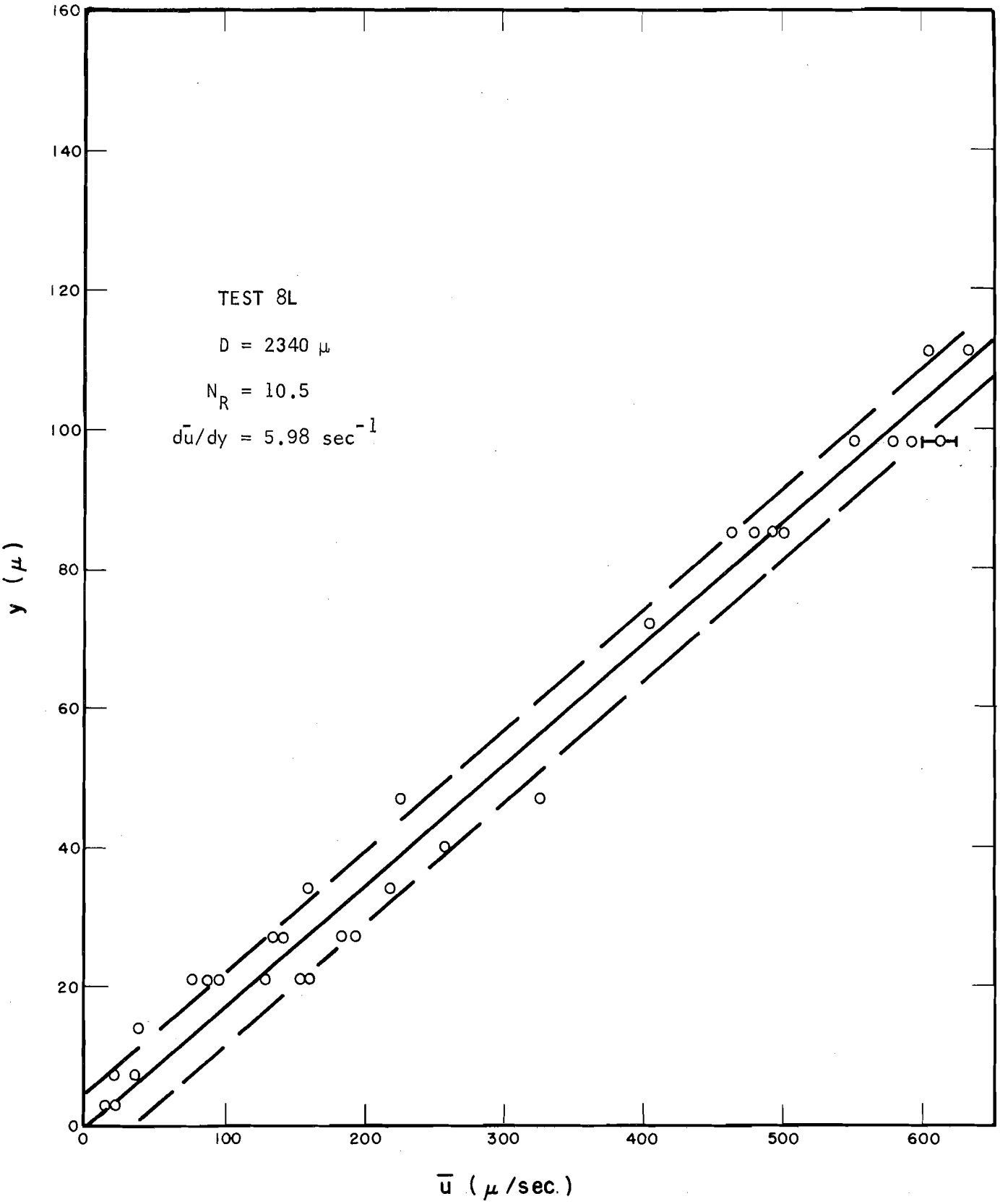

Fig. 13 — Laminar Velocity Profile

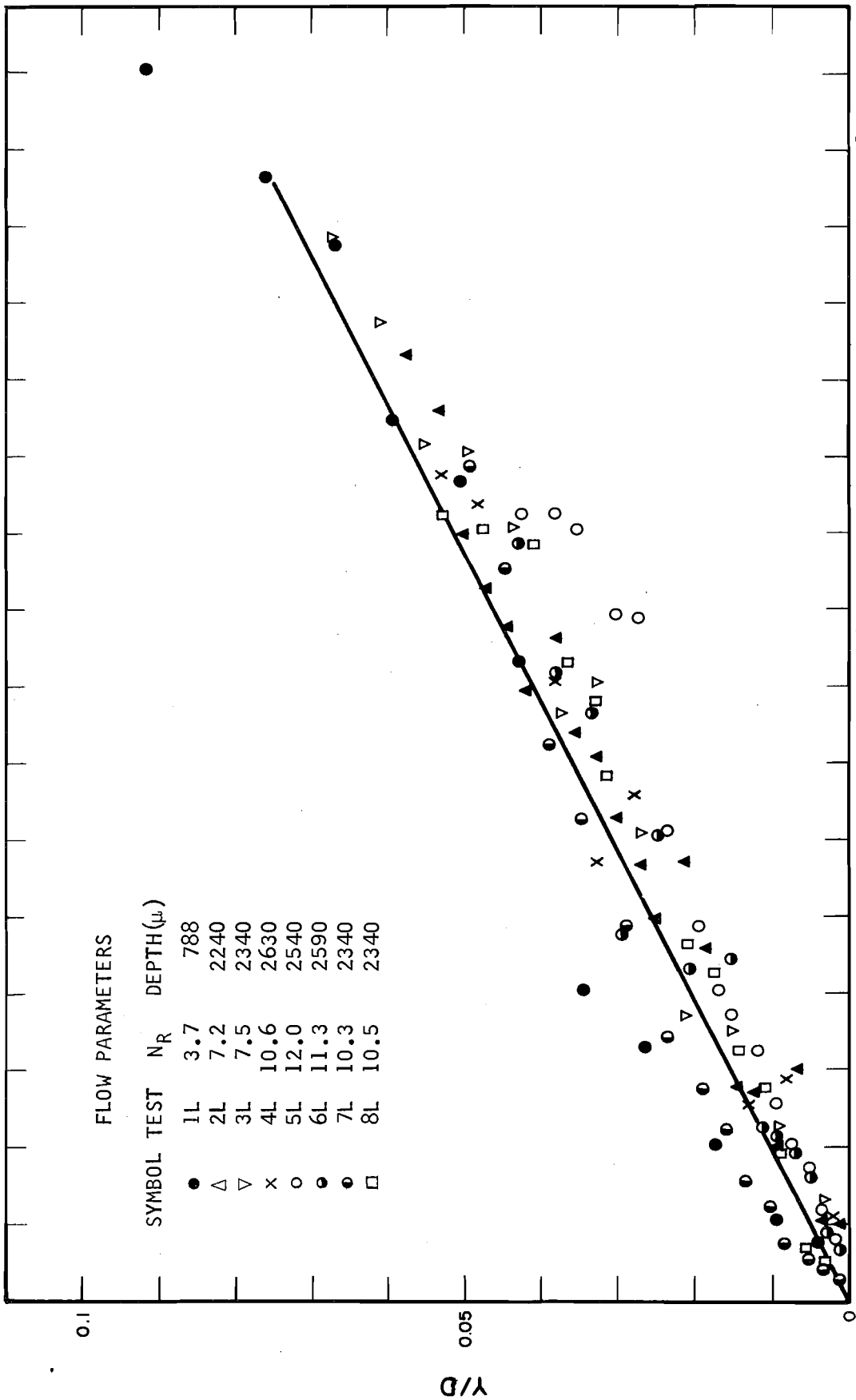

Fig. 14 — Dimensionless Laminar Velocity Profile Near Boundary

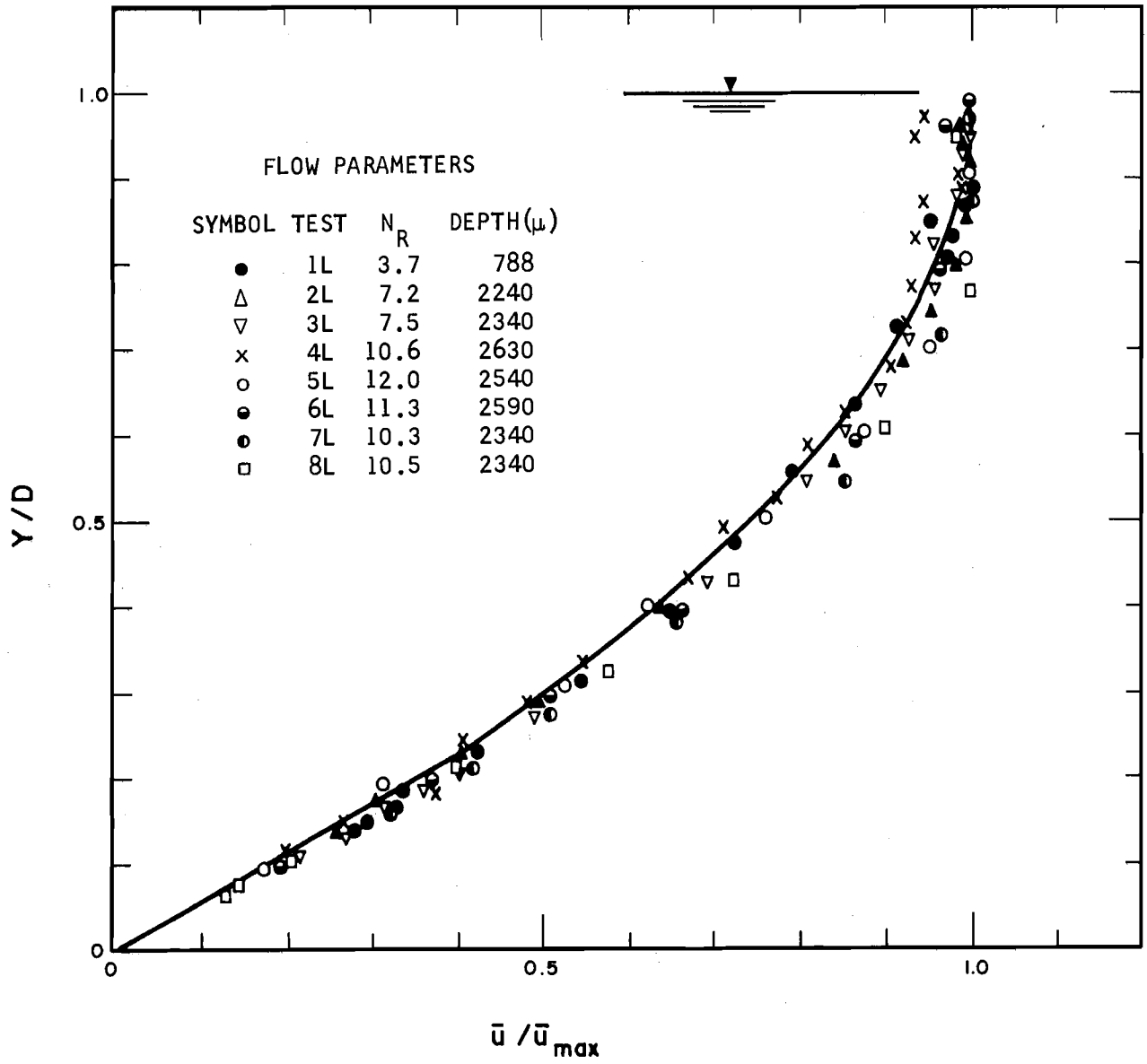

Fig. 15 — Complete Dimensionless Laminar Velocity Profile

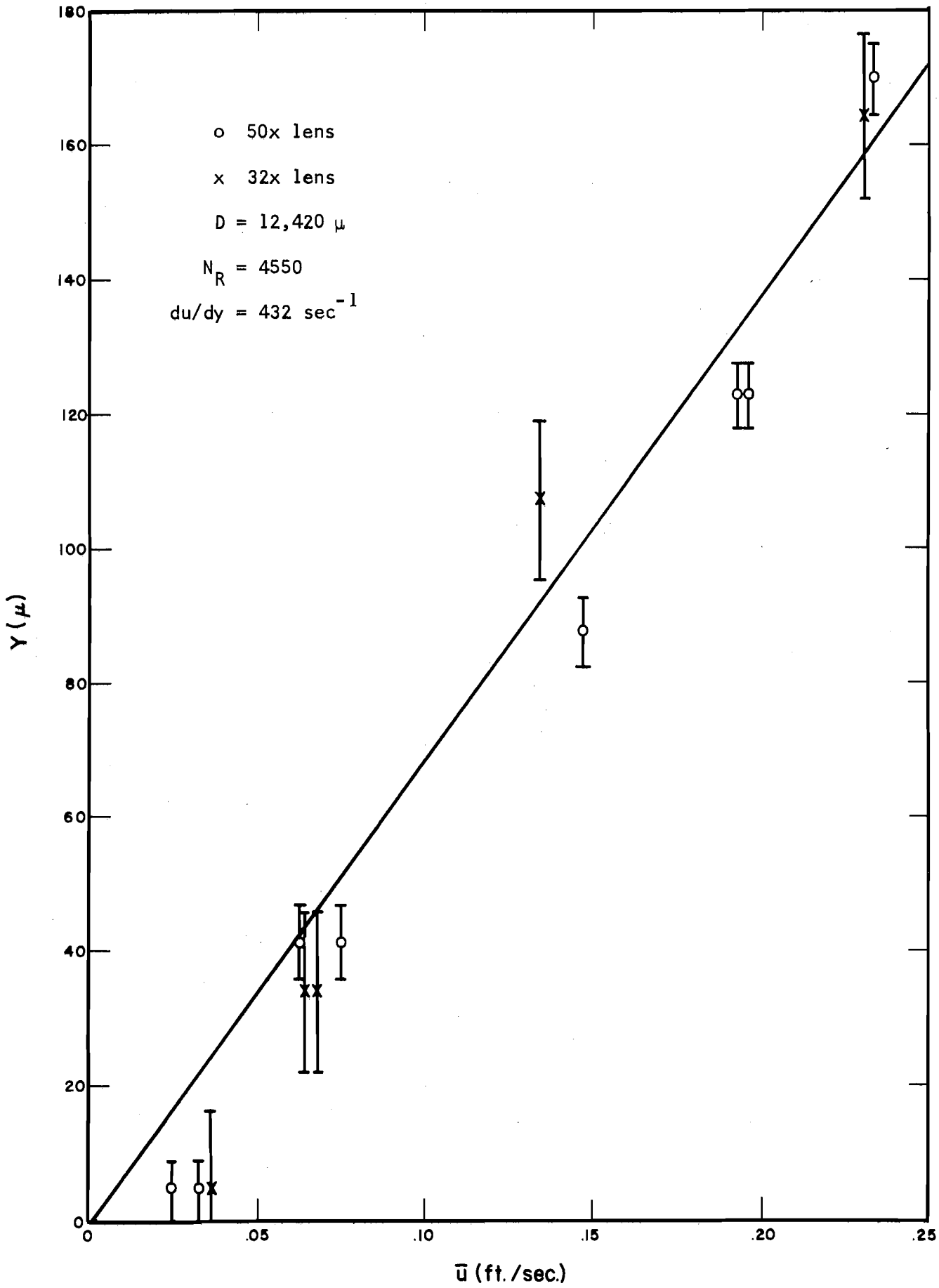

Fig. 16 — Turbulent Sublayer Velocity Profile

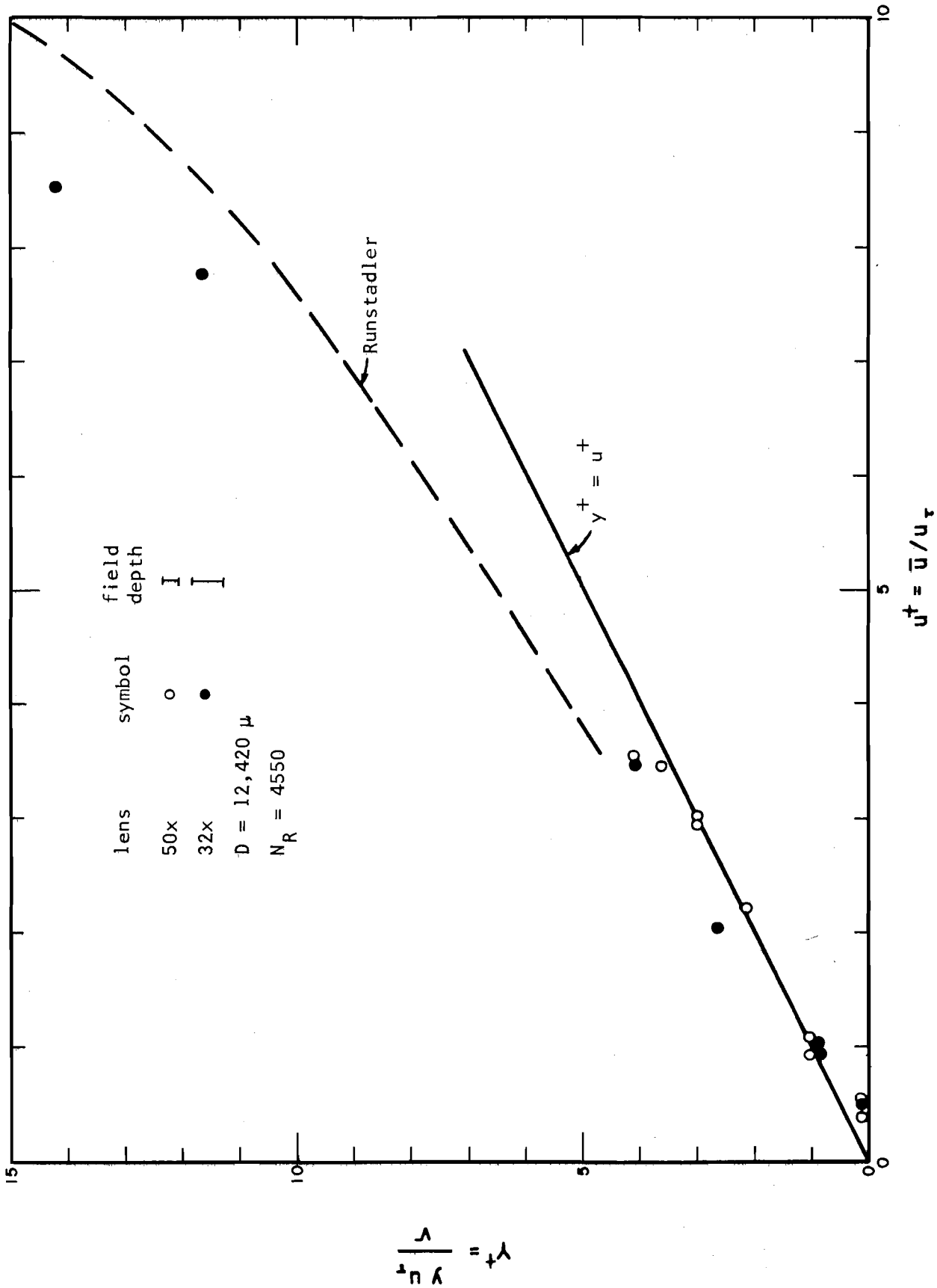

Fig. 17 — Dimensionless Turbulent Velocity Profile

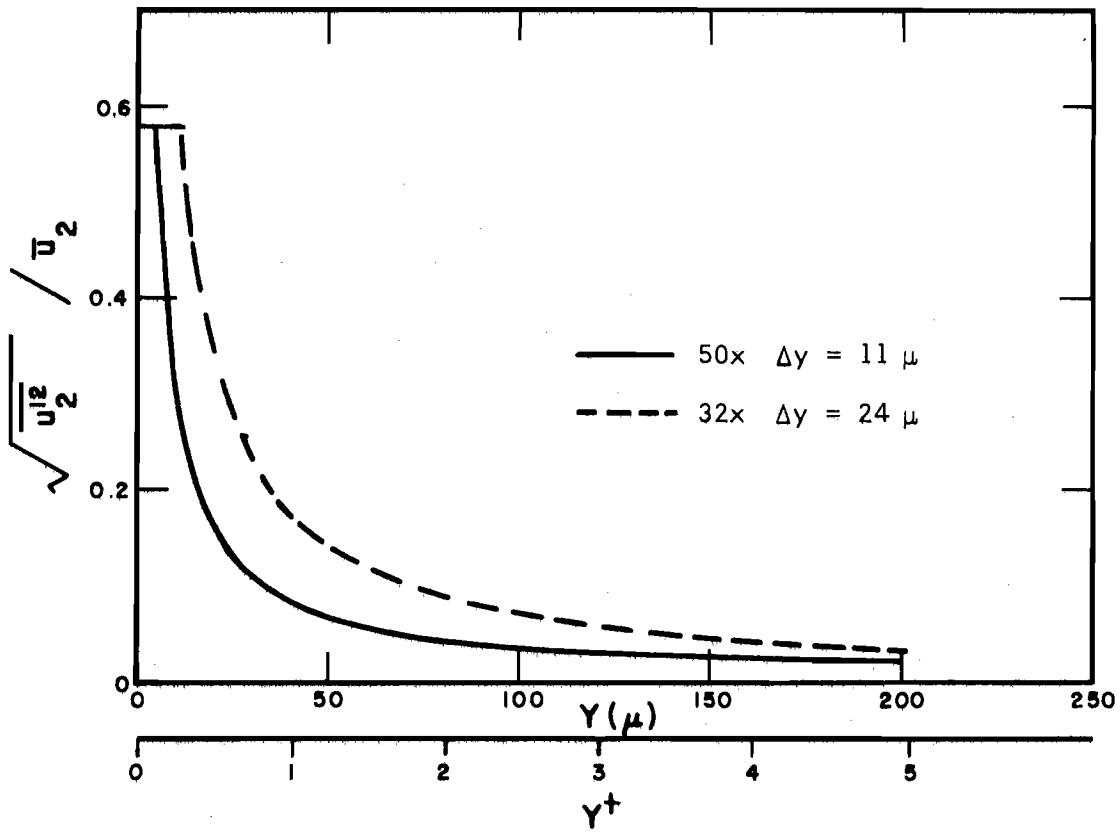

Fig. 18 — Apparent Intensity Due to Depth of Field

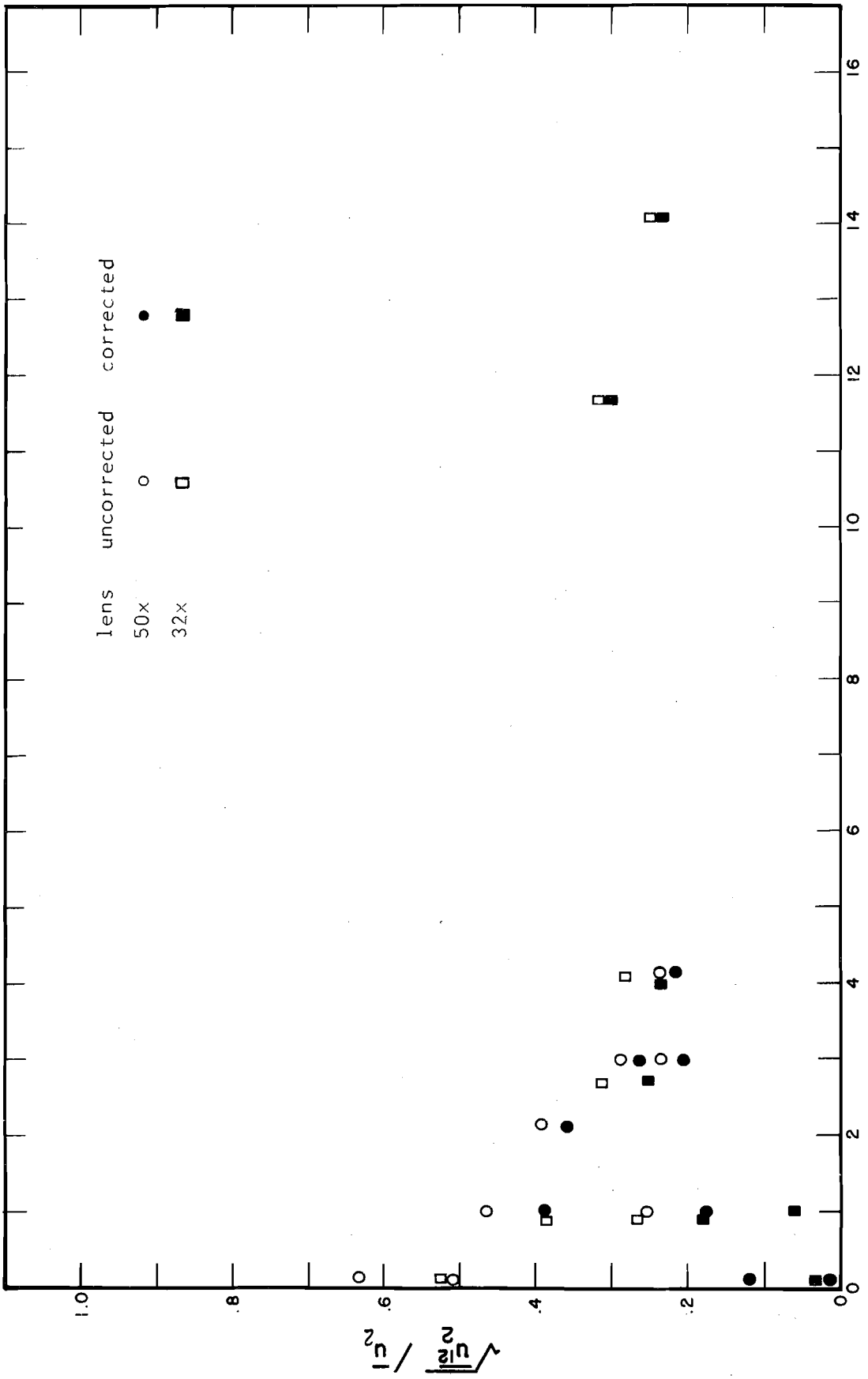

Fig. 19 — Relative Longitudinal Intensity Based on $\bar{u}_2$

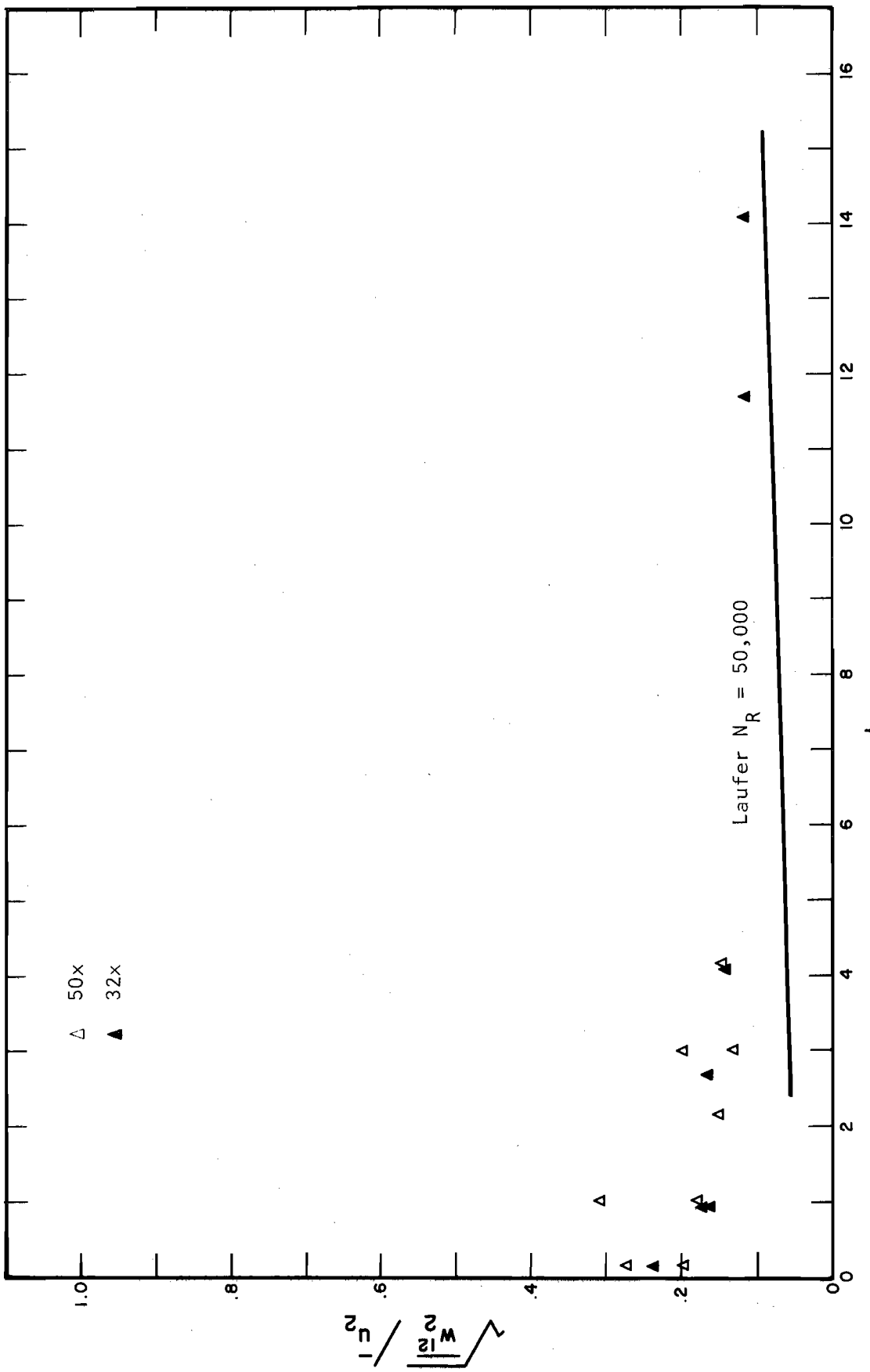

Fig. 20 — Relative Lateral Intensity Based on $\bar{u}_2$

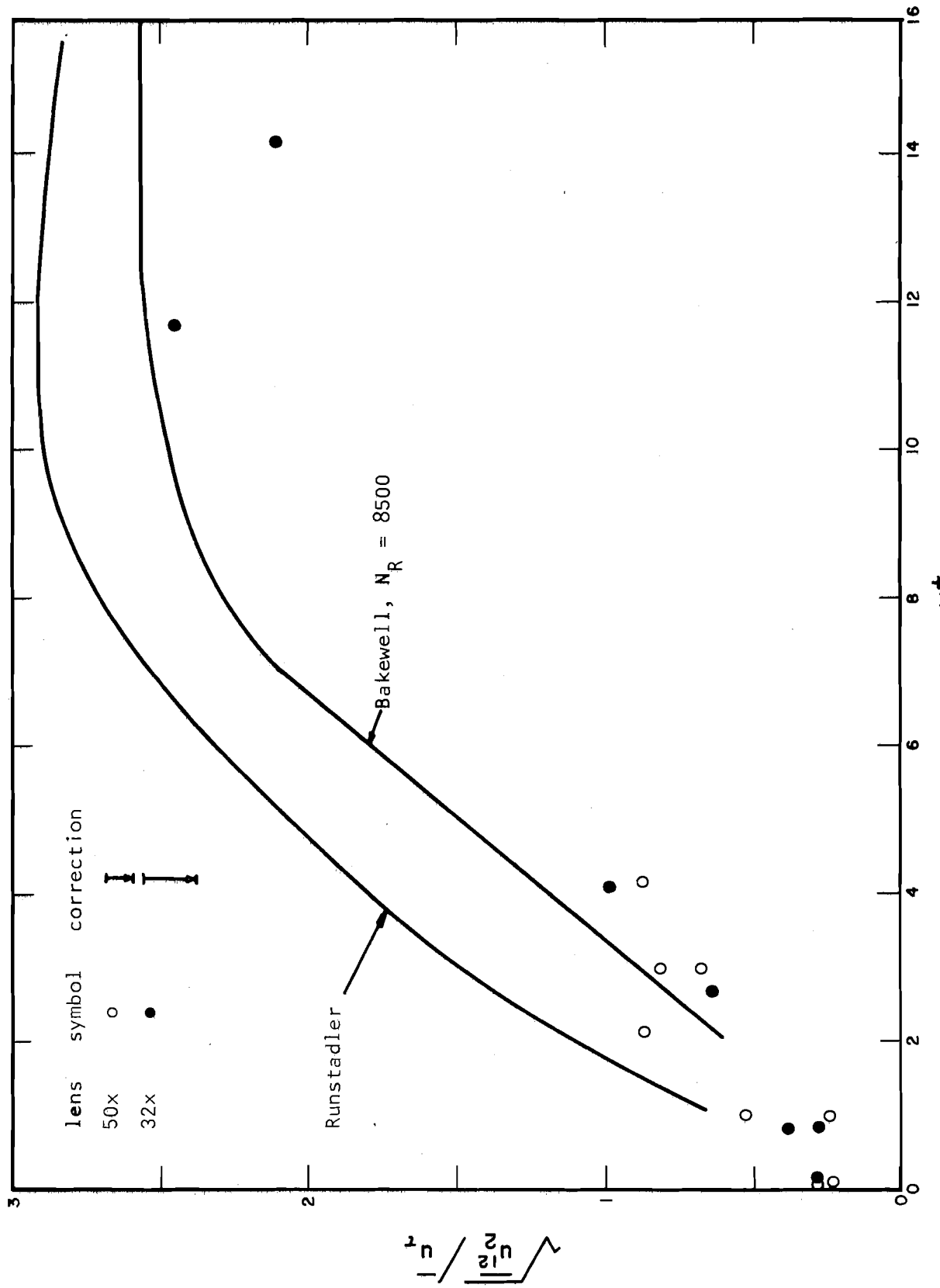

Fig. 21 — Relative Longitudinal Intensity Based on u_τ

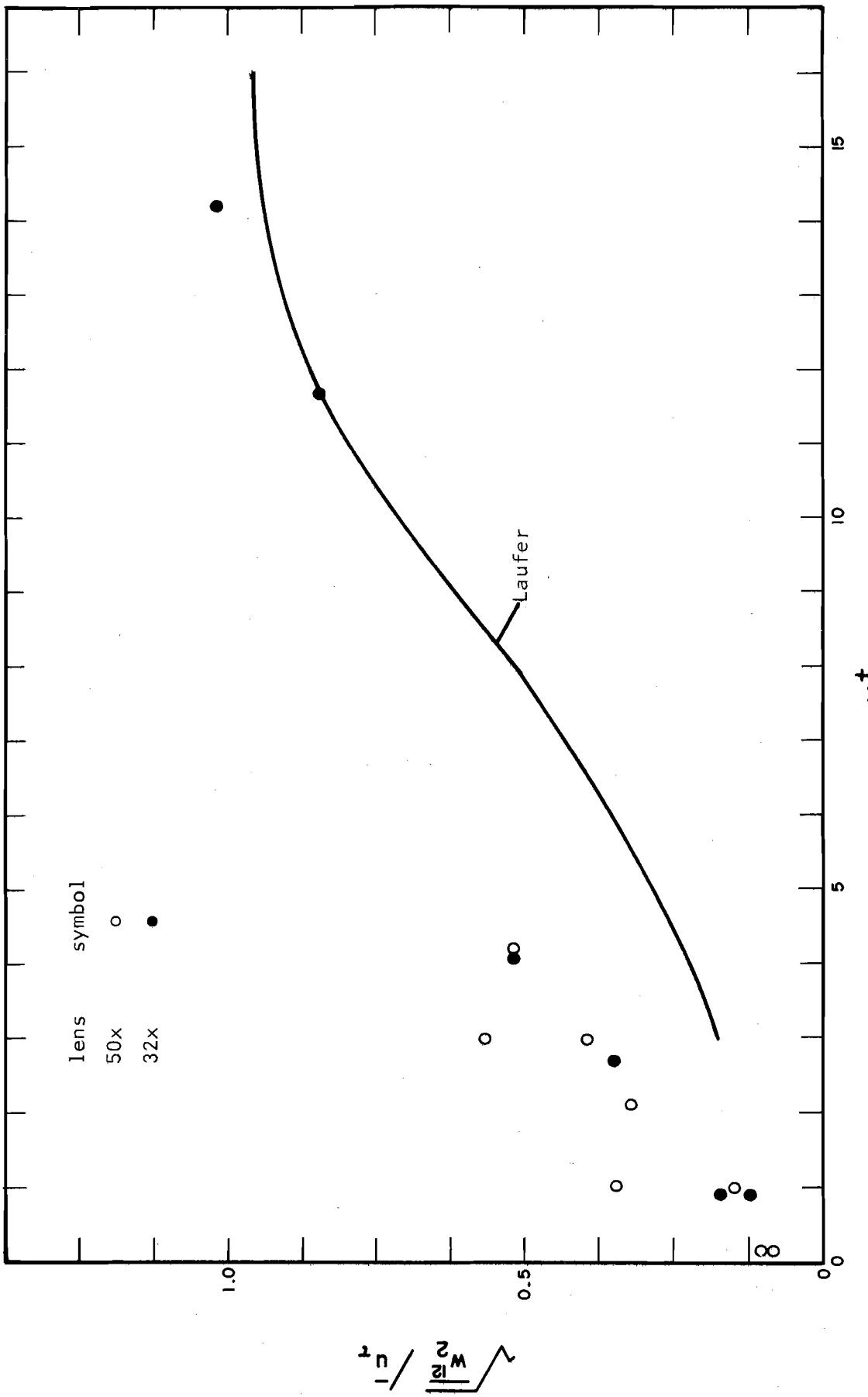

Fig. 22 — Relative Lateral Intensity Based on u_τ

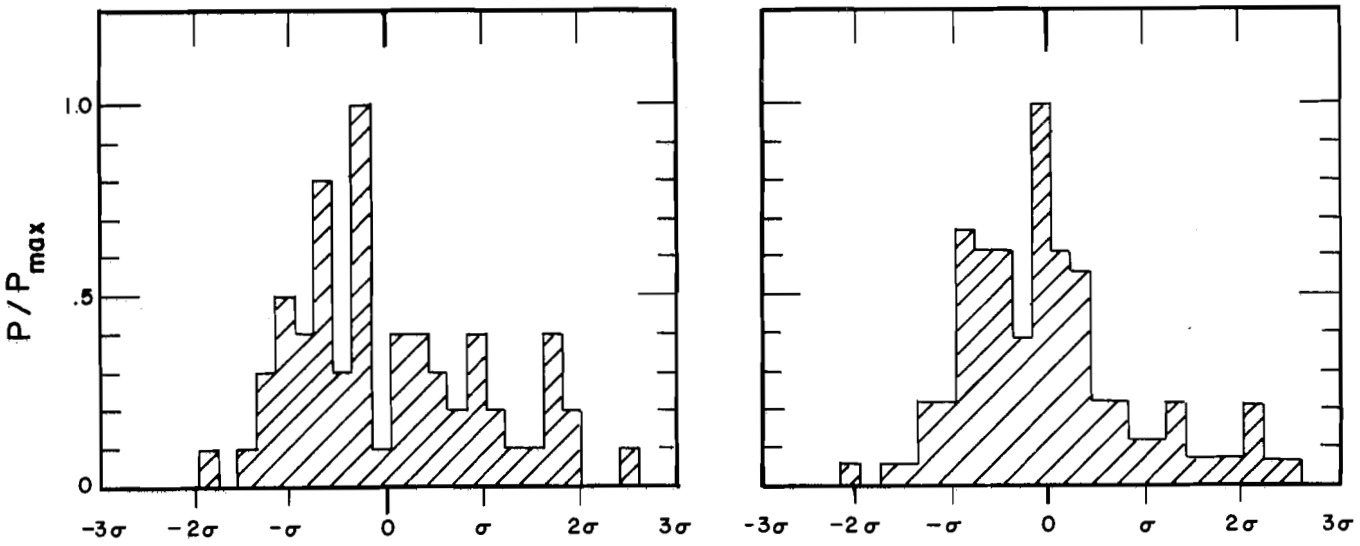

Test 1B

P_{max} = 0.1587

$\bar{u}_2$ = 0.0356 fps

σ = 0.0188 fps

y^+ = 0.11

Test 4A

P_{max} = 0.1525

$\bar{u}_2$ = 0.0751 fps

σ = 0.0352 fps

y^+ = 1.00

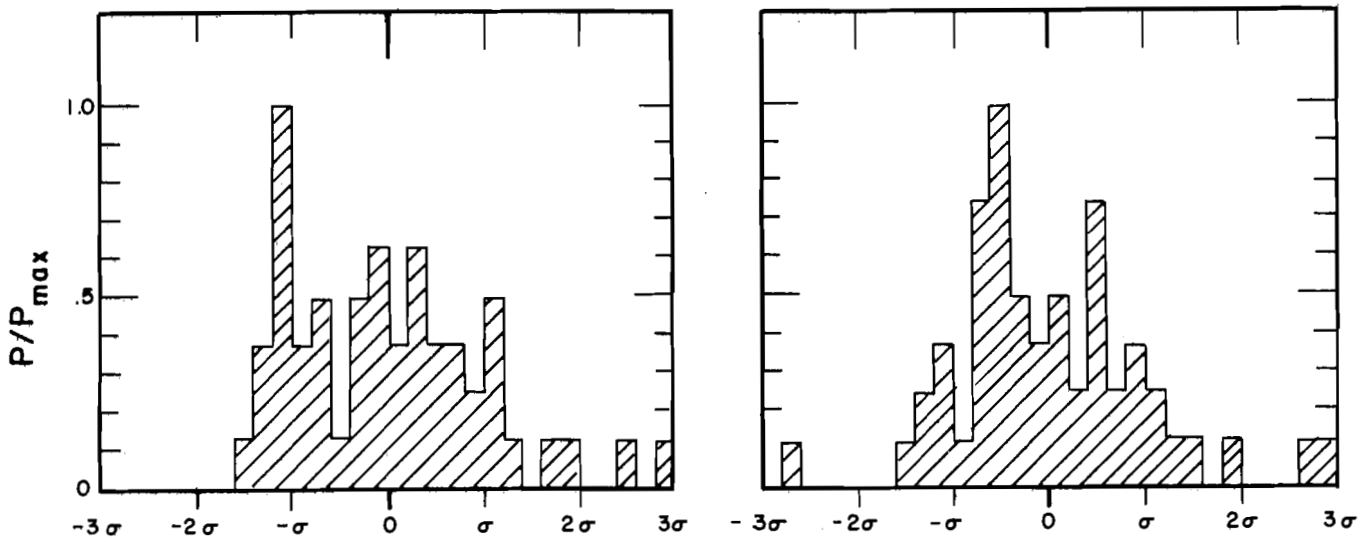

Test 8A

P_{max} = 0.1481

$\bar{u}_2$ = 0.234 fps

σ = 0.0560 fps

y^+ = 4.15

Test 7B

P_{max} = 0.1509

$\bar{u}_2$ = 0.572 fps

σ = 0.141 fps

y^+ = 14.2

Fig. 23 — Distribution of Particle Velocities

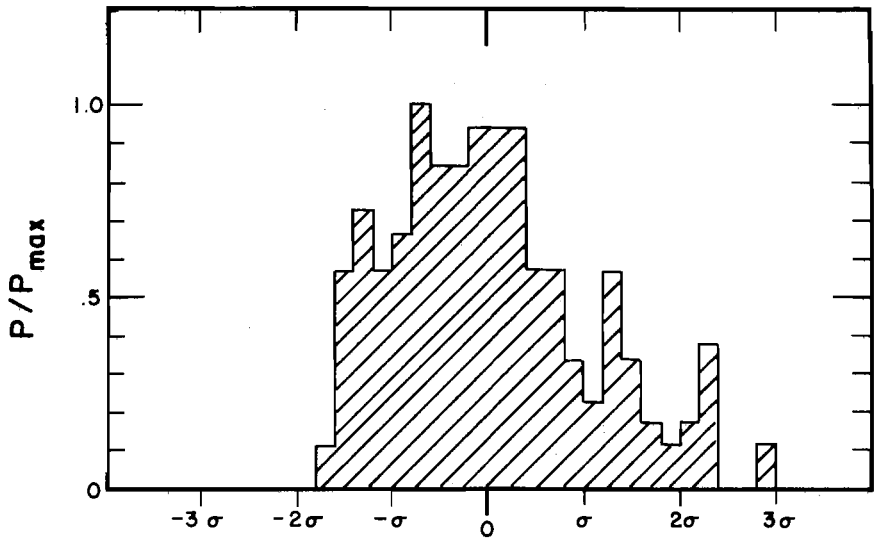

Tests 1A, 2A, 1B

P_{max} = 0.0879 σ = 0.0175 fps

$\bar{u}_2$ = 0.0303 fps y^+ = 0.10 (ave.)

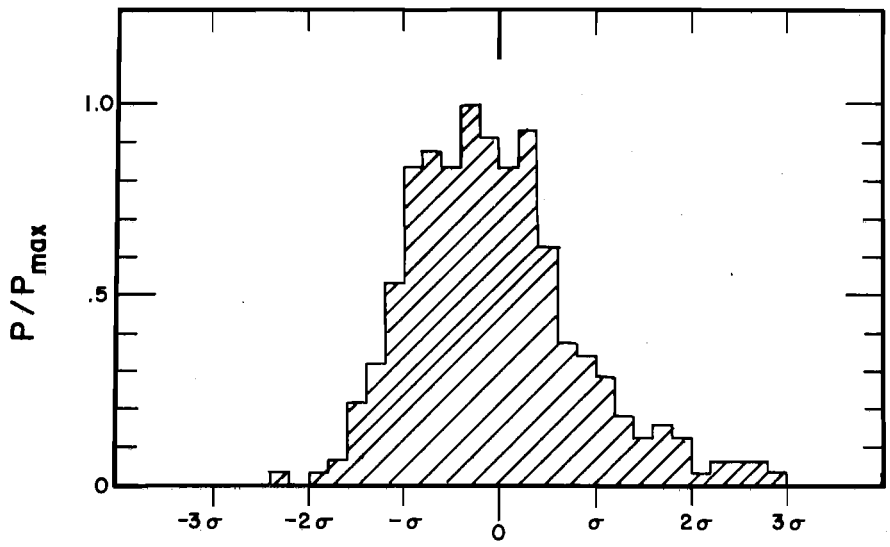

Tests 3A, 4A, 2B

P_{max} = 0.0994 σ = 0.0284 fps

$\bar{u}_2$ = 0.0677 fps y^+ = 0.95 (ave.)

Fig. 24 — Combined Distribution of Particle Velocities

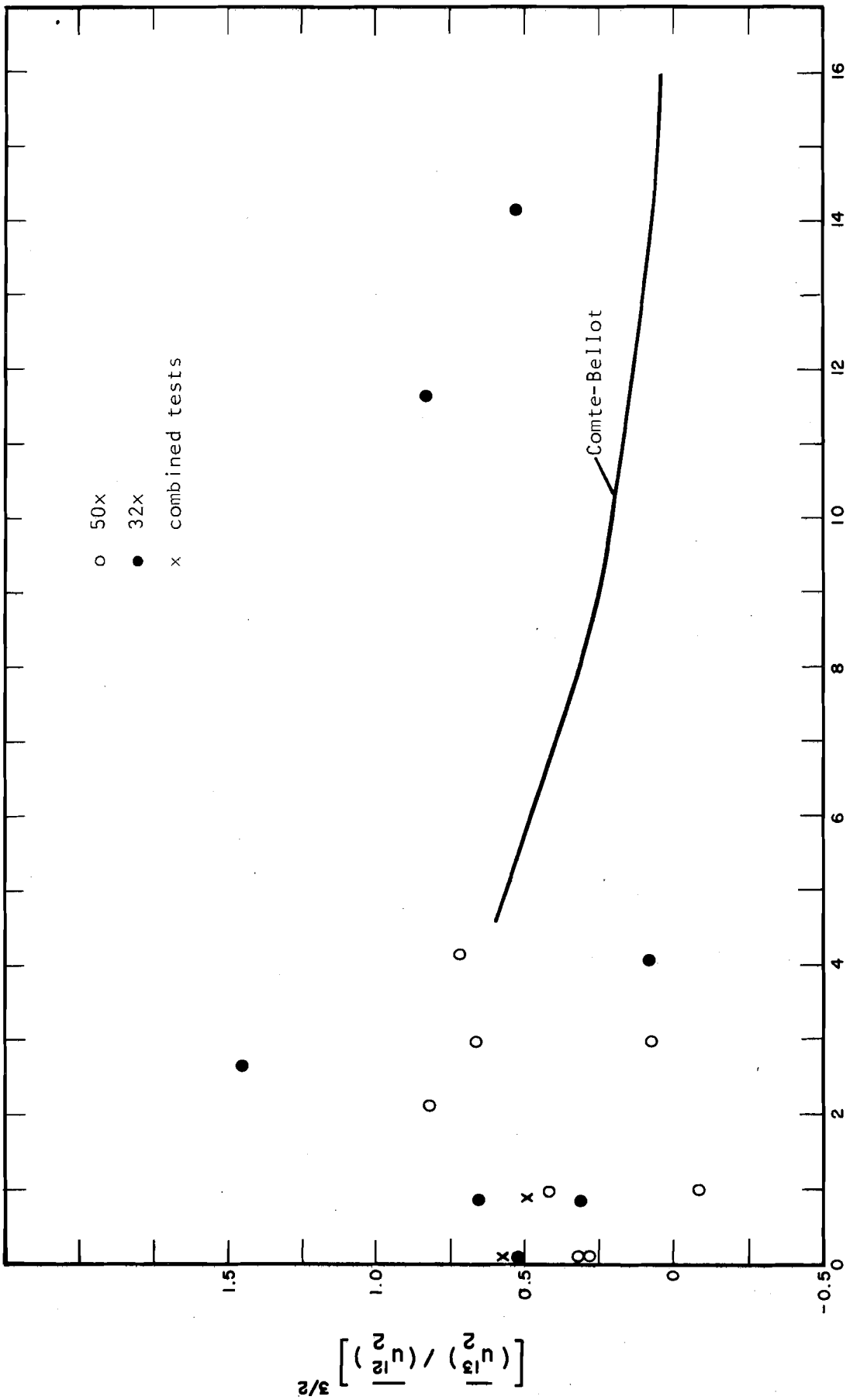

Fig. 25 — Skewness Distribution of Particle Velocities

7. CONCLUSIONS

Based on the results persented in this report and the practical experience gained, the following conclusions are made:

1. Using the high speed camera, boundary shear in the viscous sublayer can be computed with an accuracy of approximately $\pm$ 15 percent. The error is primarily the result of uncertainty in locating the focal plane and in determining the particle position within the focal plane.

2. Turbulence intensities can be determined, but uncertainty due to the depth of field increases as the boundary is approached. This reduces the value of the method as employed for this purpose.

3. The computation of the particle velocity for each frame of the film is unnecessary and leads to an average velocity which is lower than the true value. The optimum procedure would be to use the average particle velocity over a fixed time interval.

4. The time and effort required to reduce the data from the film is considerable. Feasability of direct analyses on a computor using optical acquisition methods should be investigated.

5. The proposed study of turbulent flow with the focal plane orientated normal to the boundary shows great promise since it essentially eliminates the present problems associated with the depth of field.

6. The microscopic method of studying fluid flow has great potential value in revealing the fine details of small scale local flow phenomena.

REFERENCES

1. Fage, A., and Towend, H.C.H., "An Examination of Turbulent Flow with an Ultramicroscope," Proc. Royal Soc., Vol. 135, Ser. A, 1932.

2. Fage, A. "Turbulent Flow in a Circular Pipe," Philosophical Mag., Vol. 21, Ser. 17, 1936.

3. Vogelphol, G., and Mannesmann, D., "Flow Investigation with the Aid of the Ultramicroscope," NACA TM 1109 (translation), 1946.

4. Fage, A., and Preston, J. H., "On Transition from Laminar to Turbulent Flow in the Boundary Layer," Proc. Royal Soc., Vol. 178, Ser. A, 1941.

5. Fage, A., "Studies of Boundary Layer Flow with a Fluid Motion Microscope," Nat'l. Phys. Lab., Teddington, Middlesex, England, 1955.

6. Bock. P., "Some Physical Aspects of Flow Near Surfaces," Trans. New York Aca. Sci., Ser. 111, Vol. 25, 1963.

7. Vasuki, N. C., "A Dark Field Photographic Method for Measuring Velocity Profiles," M.S. thesis, University of Delaware, 1963.

8. Carver, C. E. and Nadolink, R. H., "Measurement of Laminar Velocity Profiles with Non-Newtonian Additives Using Photomicroscopy," U. of Mass. Eng. Res. Inst. Fl. Mech. Lab. Tech. Rept. No. 1, 1965.

9. Chen, C. J. and Emrich, R. J., "Investigation of the Shock Tube Boundary Layer by a Tracer Method," Physics of Fluids, Vol. 6, No. 1, Jan., 1963.

10. Elrick, R. M., and Emrich, R. J., "Tracer Study of Pipe Flow Behavior to Within Two Microns of the Wall," Physics of Fluids, Vol. 9, No. 1, Jan., 1966.

11. Laufer, J., "Investigation of Turbulent Flow in a Two-Dimensional Channel," NACA TR 1053, 1951.

12. Laufer, J. "The Structure of Turbulence in Fully Developed Pipe Flow," NACA TR 1174, 1954.

13. Klebanoff, P. S., "Characteristics of Turbulence in a Boundary Layer with Zero Pressure Gradient," NACA TR 1247, 1955.

14. Runstadler, P. E., Kline, S. J., and Reynolds, W. C., "An Experimental Investigation of the Flow Structure of the Turbulent Boundary Layer," Report MD-8, Dept. of Mech. Engr., Stanford University, 1963.

15. Schraub, F. A. and Kline, S. J., "A Study of the Structure of the Turbulent Boundary Layer With and Without Longitudinal Pressure Gradients," Report MD-12, Dept. of Mech. Engr., Stanford University, 1965.

16. Bakewell, H. D., Jr., "An Experimental Invesitgation of the Viscous Sublayer in Turbulent Pipe Flow," Dept. of Aerospace Engr., Penn. State University, 1966.

17. Mitchell, J. E. and Hanratty, T. J., "A Study of Turbulence at a Wall Using an Electrochemical Wall Shear-Stress Meter," Jour. Fluid Mech., Vol. 26, pt. 1, 1966.

18. Tieleman, H. W., "Viscous Region of Turbulent Boundary Layer," Technical Report, Fluid Dynamics and Diffusion Laboratory, College of Engr., Colo. State University, 1967.

19. Small, S., "Experiments on the Lift and Drag of Spheres Suspended in a Low Reynolds Number Flow," Report FLD No. 11, Dept. of Mechanical Engr., Princeton University, 1963.

20. Comte-Bellot, G., "Coefficients de Dissymetrie et D'aplatissement, Spectres et Correlations in Turbulence de Conduite," Jour. de Mecanique, Vol. 2, June, 1963.